Plasma Sources Sci. Technol. **16** (2007) 656–678 doi:10.1088/0963-0252/16/3/026

Efficient models for photoionization produced by non-thermal gas discharges in air based on radiative transfer and the Helmholtz equations

A Bourdon[1], V P Pasko[2], N Y Liu[2], S Célestin[1], P Ségur[3] and E Marode[4]

[1] Ecole Centrale Paris, EM2C, UPR CNRS 288, Grande voie des vignes, 92295 Châtenay-Malabry Cedex, France
[2] Communications and Space Sciences Laboratory, Department of Electrical Engineering, The Pennsylvania State University, University Park, PA 16802, USA
[3] Université de Toulouse, LAPLACE, CNRS, INPT, UPS, 118 route de Narbonne, 31062 Toulouse Cedex 9, France
[4] Ecole Supérieure d'Électricité, LPGP, UMR CNRS 8578, Plateau du moulon, 3 rue Joliot Curie, 91192 Gif-sur-Yvette, France

E-mail: anne.bourdon@em2c.ecp.fr and vpasko@psu.edu

Received 5 April 2007, in final form 11 July 2007
Published 3 August 2007
Online at stacks.iop.org/PSST/16/656

Abstract
This paper presents formulation of computationally efficient models of photoionization produced by non-thermal gas discharges in air based on three-group Eddington and improved Eddington (SP_3) approximations to the radiative transfer equation, and on effective representation of the classic integral model for photoionization in air developed by Zheleznyak *et al* (1982) by a set of three Helmholtz differential equations. The reported formulations represent extensions of ideas advanced recently by Ségur *et al* (2006) and Luque *et al* (2007), and allow fast and accurate solution of photoionization problems at different air pressures for the range $0.1 < p_{O_2}R < 150$ Torr cm, where p_{O_2} is the partial pressure of molecular oxygen in air in units of Torr ($p_{O_2} = 150$ Torr at atmospheric pressure) and R in cm is an effective geometrical size of the physical system of interest. The presented formulations can be extended to other gases and gas mixtures subject to availability of related emission, absorption and photoionization coefficients. The validity of the developed models is demonstrated by performing direct comparisons of the results from these models and results obtained from the classic integral model. Specific validation comparisons are presented for a set of artificial sources of photoionizing radiation with different Gaussian dimensions, and for a realistic problem involving development of a double-headed streamer at ground pressure. The reported results demonstrate the importance of accurate definition of the boundary conditions for the photoionization production rate for the solution of second order partial differential equations involved in the Eddington, SP_3 and the Helmholtz formulations. The specific algorithms derived from the classic photoionization model of Zheleznyak *et al* (1982), allowing accurate calculations of boundary conditions for differential equations involved in all three new models described in this paper, are presented. It is noted that the accurate formulation of boundary conditions represents an important task needed for a successful extension of the proposed formulations to two- and three-dimensional physical systems with obstacles of complex geometry (i.e. electrodes, dust particles, aerosols, etc), which are opaque for the photoionizing UV photons.

1. Introduction

Plasma discharges at atmospheric pressure have received renewed attention in recent years due to their ability to enhance the reactivity of a variety of gas flows for applications ranging from surface treatment to flame stabilization and ignition. In air at atmospheric pressure, discharges usually take the form of filamentary streamers. These discharges are characterized by a high electron concentration in a narrow filament and produce high concentrations of chemically active species that can effectively enhance the reactivity to a level sufficient for many applications of interest (e.g. van Veldhuizen 2000). The examples of related applications include ozone production, pollution control, surface processing (Raizer 1991, van Veldhuizen 2000 and references cited therein), and triggering of combustion in spark ignition engines

(Tardiveau *et al* 2001, Tardiveau and Marode 2003). An excellent recent review of various applications of streamers is provided by Ebert *et al* (2006).

The concept of streamer discharges was introduced in the 1930s to explain naturally occurring spark discharges (Loeb and Meek 1940). Streamers are regarded as the precursor of spark discharges. They can initiate spark discharges in relatively short (several cm) gaps at near ground pressures in air. In ground air pressure applications a typical transverse scale of individual streamer filaments is a fraction of a millimetre (e.g. Bastien and Marode 1979, Pancheshnyi *et al* 2005, Briels *et al* 2005), and may be substantially wider depending on the circuit and the peak applied voltage characteristics of a particular experiment (Briels *et al* 2006). Lightning is a natural phenomenon directly related to streamer discharges. A streamer zone consisting of many highly-branched streamers usually precedes leader channels initiating lightning discharges in large volumes at near ground pressure (Raizer 1991, p 364).

About two decades ago, large-scale electrical discharges were discovered in the mesosphere and lower ionosphere above large thunderstorms, which are now commonly referred to as sprites (e.g. Franz *et al* 1990, Sentman *et al* 1995, Stanley *et al* 1999, Neubert 2003, Lyons 2006). Recent telescopic imaging of sprites at standard video rates (i.e. with $\sim$16 ms time resolution) revealed an amazing variety of generally vertical fine structure with transverse spatial scales ranging from tens to a few hundred meters (Gerken *et al* 2000, Gerken and Inan 2002, 2003, 2005). The most recent continuous high-speed video recordings of sprites at $\sim$10 000 frames per second further confirm that filamentary structures are abundantly present in sprite discharges (Cummer *et al* 2006, McHarg *et al* 2007, Stenbaek-Nielsen *et al* 2007). It is interesting to note that the filamentary structures observed in sprites are the same phenomenon as streamer discharges at atmospheric pressure only scaled by reduced air density at higher altitudes (Pasko *et al* 1998, Liu and Pasko 2004, 2005, 2006, Liu *et al* 2006). An overview of the physical mechanism and molecular physics aspects of sprite discharges in comparison with laboratory discharges can be found in Pasko (2007).

Various models have been developed to study propagation of streamers (see Raizer 1991 p 352 and Bazelyan and Raizer 1998 p 176). Well before numerical modelling techniques were applied to this field of research, two simple models of the streamer process had been proposed to qualitatively study streamers: an isolated head model and a model treating the streamer channel as ideally conducting. The first one considers the head of a streamer as a charged sphere. As it moves, it leaves behind a quasi-neutral ionized channel. However, the conductivity of the channel is assumed to be negligibly low and the head is not connected to the anode (Raizer 1991, p 352). The second one assumes that the conductivity of the streamer channel is infinite, and its surface is equipotential. The charges induced by the external field are distributed along the surface (Raizer 1991, p 356). There has been no answer to the question of which model is valid until recently. Numerical simulation results from a two-dimensional streamer model based on a diffusion–drift approximation have indicated that the streamer channel has finite conductivity (Dhali and Williams 1987). Since then, the streamer model proposed by Dhali and Williams (1987) has been improved and is now widely used in the modeling of streamer propagation for many purposes (e.g. Vitello *et al* 1994, Babaeva and Naidis 1997, Kulikovsky 2000, Pancheshnyi *et al* 2001, Arrayas *et al* 2002).

It is generally recognized that streamers are driven by highly nonlinear space charge waves (e.g. Raizer 1991, p 327), and develop in a self-consistent manner. Streamers are known to have two polarities: positive (cathode-directed) and negative (anode-directed), defined by the sign of the charge in their heads. The positive streamer propagates against the direction of the electron drift, while the negative one moves in the same direction as the electron drift. The photoionization produced by UV photons originating from a region of high electric field in the streamer head is responsible for creation of seed electrons in front of the head of a propagating streamer, and is believed to play a critical role in the spatial advancement of streamers of both polarities (e.g. Babaeva and Naidis 1997, Rocco *et al* 2002, Kulikovsky 2000, Pancheshnyi *et al* 2001, Luque *et al* 2007).

In a diffusion–drift or hydrodynamic-like approach to streamer modelling, the motion of electrons, ions and excited molecules is governed by continuity equations coupled to Poisson's equation (e.g. Dhali and Williams 1987). The photoionization process is taken into account through a source term which is added to the continuity equations of electrons and ions. During early attempts of numerical simulations of streamers, the photoionization term was ignored and the pre-ionization needed for stable advancement of streamers of both polarities was provided by introducing a uniform neutral background ionization of the gas (e.g. Dhali and Williams 1987, Vitello *et al* 1994). In the current literature, the photoionization term is usually calculated using integral models with coefficients based either on the classical experiments of Penney and Hummert 1970 and Teich 1967 (e.g. Wu and Kunhardt 1988, Kunhardt and Tzeng 1988, Morrow and Lowke 1997), or on the description proposed by Zheleznyak *et al* 1982 for air (e.g. Babaeva and Naidis 1997, Kulikovsky 2000, Pancheshnyi *et al* 2001, Liu and Pasko 2004, 2006).

The accurate and efficient evaluation of the effects of photoionization remains one of the most challenging tasks in streamer modelling. For the integral approach mentioned above, the calculation of the photoionization source term at a given point of the volume studied requires a quadrature over the complete volume of the discharge. Therefore, the calculation of the photoionization source term in streamer discharges is computationally expensive. To accelerate the simulation of streamers, different approximations are proposed in the literature to reduce the computation time spent on calculation of the photoionization source term (Kulikovsky 2000, Pancheshnyi *et al* 2001, Hallac *et al* 2003). Kulikovsky (2000) proposed to confine the emitting volume of the photoionizing radiation to a small cylinder around the main axis of the discharge and to divide it into small rings. For a two-dimensional modeling of streamers assuming cylindrical symmetry, the effects of an emitting ring at a point of interest can be effectively characterized by their relative locations (described by

a geometric factor in Kulikovsky (2000)). This geometric factor only needs to be calculated once before the simulation for a specific computational geometry and can be repeatedly reused in the simulations. In Kulikovsky (2000) and Hallac *et al* (2003) photoionization is calculated on a coarse grid and interpolation is used to obtain needed values on the main grid. Finally, in Pancheshnyi *et al* (2001) calculations are carried out in a small area around the streamer head. Pancheshnyi *et al* (2001) also compared the streamer discharge characteristics obtained by using spatially uniform background pre-ionization level with those obtained by the integral model. They found that although it is possible to obtain an agreement of some characteristics by varying the pre-ionization level, the agreement cannot be reached for all the characteristics at a given pre-ionization level. We note that all the approximate models reviewed above reduce the computation time to a certain degree but the accuracy of these models has not yet been rigorously evaluated and demonstrated in the existing literature.

Recently, two different approaches to calculate the photoionization term have been proposed to avoid the calculation of the global quadrature over the simulation domain. The first approach was tested a few years ago (Djermoune *et al* 1995a, 1995b) and improved recently (Ségur *et al* 2006). This method is based on the direct numerical solution of an improved Eddington approximation of the radiative transfer equation. The second approach has been proposed recently by Luque *et al* (2007). These authors proposed to approximate the absorption function of the gas in order to transform the integral expression of the photoionization term into a set of Helmholtz differential equations.

In this paper, we discuss several models based on the differential equation approach currently proposed in the literature for the calculation of the photoionization term (Ségur *et al* 2006, Luque *et al* 2007), and develop improved models based on the same principles by more accurately accounting for the spectral dependence of the photoionization. The validity and range of applicability of the developed models are demonstrated by performing direct comparisons of the results from these models and results obtained from the classic integral model of Zheleznyak *et al* (1982). Specific validation comparisons are presented for a set of artificial sources of photoionizing radiation with different Gaussian dimensions and for a realistic problem involving development of a double-headed streamer at ground pressure.

2. Model formulation

2.1. Classical integral model for photoionization in air

In the widely used model derived by Zheleznyak *et al* (Zheleznyak *et al* 1982, Liu and Pasko 2004, Naidis 2006) for photoionization in air, the photoionization rate at point of observation $\vec{r}$ due to source points emitting photoionizing UV photons at $\vec{r}\,'$ is

$$S_{\mathrm{ph}}(\vec{r}) = \iiint_{V'} \frac{I(\vec{r}')g(R)}{4\pi R^2}\,\mathrm{d}V', \tag{1}$$

where $R = |\vec{r} - \vec{r}'|$. In this model, to simplify calculations, the production of photons is assumed to be proportional to the ionization production rate S_{i}, and then $I(\vec{r})$ is given by

$$I(\vec{r}) = \xi\frac{n_u(\vec{r})}{\tau_u} = \frac{p_{\mathrm{q}}}{p + p_{\mathrm{q}}}\,\xi\frac{\nu_u}{\nu_{\mathrm{i}}}S_{\mathrm{i}}(\vec{r}), \tag{2}$$

where ξ is the photoionization efficiency, $n_u(\vec{r})$ is the density of the radiative excited species u, the ratio $p_{\mathrm{q}}/(p + p_{\mathrm{q}})$ is a quenching factor, τ_u is the lifetime of the excited state u accounting for the effects of spontaneous emission and quenching (i.e. $\tau_u = p_q/(A_u(p+p_q))$, where A_u is the Einstein coefficient), ν_u is the electron impact excitation frequency for level u, and $S_i = \nu_i n_{\mathrm{e}}$, where n_{e} is the electron number density and ν_{i} is the ionization frequency. The function $g(R)$ in (1) is defined by

$$\frac{g(R)}{p_{\mathrm{O_2}}} = \frac{\exp(-\chi_{\min}p_{\mathrm{O_2}}R) - \exp(-\chi_{\max}p_{\mathrm{O_2}}R)}{p_{\mathrm{O_2}}R\,\ln(\chi_{\max}/\chi_{\min})}, \tag{3}$$

where $\chi_{\min} = 0.035\,\mathrm{Torr}^{-1}\,\mathrm{cm}^{-1}$, $\chi_{\max} = 2\,\mathrm{Torr}^{-1}\,\mathrm{cm}^{-1}$ and where $p_{\mathrm{O_2}}$ is the partial pressure of molecular oxygen (=150 Torr at atmospheric pressure). We note that in equation (3) we divided $g(R)$ by $p_{\mathrm{O_2}}$ to make the result conveniently dependent on the product $p_{\mathrm{O_2}}R$, which is an important parameter for photoionization in N_2–O_2 mixtures as shown by Zheleznyak *et al* (1982). The dependence of the right-hand side of equation (3) on the $p_{\mathrm{O_2}}R$ product makes it easily scalable to different pressures.

The above described model has typically been employed in a cylindrical coordinate system to model the dynamics of two-dimensional azimuthally symmetric streamers. Following the approach proposed by Kulikovsky (2000), the emitting volume in this kind of coordinate system (r, ϕ, z) is divided into small rings centred at the symmetry axis (figure 1(*a*)), and the photoionization rate at point of observation (r, z) due to all source rings $(r_{\mathrm{s}}, z_{\mathrm{s}})$ in $\mathrm{cm}^{-3}\,\mathrm{s}^{-1}$ is

$$S_{\mathrm{ph}}(r, z) = \int \mathrm{d}r_{\mathrm{s}} \int \mathrm{d}z_{\mathrm{s}} I(r_{\mathrm{s}}, z_{\mathrm{s}}) M_{\mathrm{ph}}(r, r_{\mathrm{s}}, |z - z_{\mathrm{s}}|). \tag{4}$$

In equation (4) the integration is performed over all source regions with significant production of photoionizing radiation and the function M_{ph} is defined as

$$M_{\mathrm{ph}}(r, r_{\mathrm{s}}, |z - z_{\mathrm{s}}|) = \frac{r_{\mathrm{s}}}{4\pi}\int_0^{2\pi} \frac{g[R(\phi_{\mathrm{s}})]}{R(\phi_{\mathrm{s}})^2}\mathrm{d}\phi_{\mathrm{s}}, \tag{5}$$

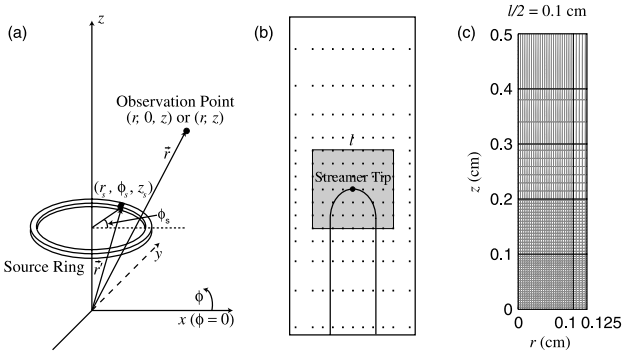

Figure 1. (*a*) Elementary emitting volume (ring) for photoionization calculations. (*b*) Schematic illustration of the inhomogeneous grid for efficient photoionization calculations using the integral model. (*c*) Illustration of an inhomogeneous grid system for acceleration of photoionization calculations using the integral model.

where $R(\phi_s) = |\vec{r} - \vec{r}'| = [r_s^2 + r^2 + (z - z_s)^2 - 2rr_s\cos(\phi_s)]^{\frac{1}{2}}$.

The geometric factor M_{ph} depends on r, r_s and $|z - z_s|$, and it is possible to calculate M_{ph} once and store it as a three-dimensional array, which can be repeatedly reused for computation of S_{ph} at each time step in the simulation. Even with this simplification the integral model for photoionization is computationally very expensive because a two-dimensional integration (equation (4)) has to be carried out for each observation point (r, z). To further improve the computation efficiency, a straightforward technique of using a coarse grid for photoionization calculation instead of the main grid can be employed. A homogeneous coarse grid is utilized for this purpose in Kulikovsky (2000) and Hallac *et al* (2003).

A more accurate and efficient grid system is an inhomogeneous one with fine resolution around the streamer head and coarse resolution in the region away from the head as shown schematically in figure 1(*b*). In this approach every time when the photoionization is calculated, a new grid is generated with the origin at the streamer tip, where the electric field is maximum. The photoionizing emission source is assumed to be confined in the shaded region shown in figure 1(*b*). The value of S_{ph} at each point of the new grid is calculated using equation (4) by accounting for the sources in the shaded region only. A linear or exponential interpolation is used to obtain S_{ph} at the main grid points. The M_{ph} required for integration (4) still needs to be calculated only once and stored in a three-dimensional array for a repeated use.

Figure 1(*c*) provides an example of practical implementation of the above discussed ideas. If the size of the simulation domain is $0.5 \times 0.125\ cm^2$, a grid for the calculation of M_{ph} can be set up as shown in figure 1(*c*), where the effective diameter of the shaded region shown in figure 1(*b*) is assumed to be $l = 0.2$ cm. In the z direction the simulation domain is divided into equal intervals with length $l/2 = 0.1$ cm. The grid size in each of these intervals is constant, and increases exponentially with the distance from the origin from one interval to the next. If the grid size in a particular interval becomes greater than the interval itself $(l/2)$, then $l/2$ is used as the grid size instead, as shown, for example for the interval from $z = 0.4$ to 0.5 cm in figure 1(*c*). The grid in the r direction is generated following the same procedure. M_{ph} can then be calculated on this grid using equation (5). The grid for the problem geometry shown in figure 1(*b*) can be generated by following the same ideas with the origin placed at the streamer tip and with the $l/2$ intervals with reduced grid resolution extending in both positive and negative z directions from the shaded region. The calculation of the contribution to $S_{ph}(r, z)$ due to a source ring at (r_s, z_s) is significantly accelerated by a simple call of the corresponding pre-calculated element of the three-dimensional matrix $M_{ph}(r, r_s, |z - z_s|)$. Finally, the contributions from all the rings constituting the shaded source shown in figure 1(*b*) are summed up to obtain the total $S_{ph}(r, z)$.

The integral approach with variable size grids based on the Zheleznyak *et al* (1982) model outlined above is used for the streamer calculations reported in section 3.2 of this paper. It should be noted that for a double-headed streamer reported in section 3.2, there are two grid systems generated with the origin of each grid system positioned at the tip of the corresponding streamer head. However, the same pre-calculated M_{ph} matrix is used for both heads.

2.2. *Two and three-exponential Helmholtz models for photoionization in air*

Luque *et al* (2007) have recently proposed a novel approach allowing to effectively replace the calculation of integral (1) of the classic photoionization model with a solution of a set of Helmholtz differential equations, which can be very efficiently solved using well-developed techniques available for solution of the elliptic partial differential equations. In terms of the notation adopted in this paper the approach proposed by Luque *et al* (2007) involves fitting of the $g(R)/R$ ratio in (1) with a sum of exponential functions leading to a set of integrals, each of which can effectively be interpreted as an integral solution of a separate Helmholtz differential equation. After this equivalent representation is established the problem can be solved by solving the set of Helmholtz differential equations, instead of direct evaluation of integrals. However, the two-exponential fit provided in Luque *et al* (2007) is applied to low pressure experimental data of Penney and Hummert (1970) effectively corresponding to the function $g(R)$, rather than to $g(R)/R$ required for the correct solution of the problem. In this section we present the correct solution of this problem using two and three-exponential fits. In section 3.1 we demonstrate that the two-exponential fit is generally not sufficient and the three-exponential fit is needed for obtaining the accurate solution of the problem for a full range of $p_{O_2}R$ values in which the Zheleznyak *et al* (1982) photoionization model remains valid.

We note that the Zheleznyak *et al* (1982) photoionization model, discussed in the previous section, is formulated using experimental data obtained at low pressure (Penney and Hummert 1970, Teich 1967) and agrees well with the results of more recent experiments at atmospheric pressure (Naidis 2006 and references cited therein). Therefore, in contrast to Luque *et al* (2007) in our derivation below we do not employ the low pressure data of Penney and Hummert (1970), but rather formulate the two and three-exponential Helmholtz models using the $g(R)$ function (3) appearing in the classic integral model for photoionization in air (Zheleznyak *et al* 1982).

The function $S_{ph}(\vec{r})$ given by (1) can be represented in the form

$$S_{ph}(\vec{r}) = \sum_j S_{ph}^j(\vec{r}) \tag{6}$$

with terms

$$S_{ph}^j(\vec{r}) = \iiint_{V'} \frac{I(\vec{r}')A_j p_{O_2}^2 e^{-\lambda_j p_{O_2} R}}{4\pi R}\, dV' \tag{7}$$

satisfying the Helmholtz differential equations

$$\nabla^2 S_{ph}^j(\vec{r}) - (\lambda_j p_{O_2})^2 S_{ph}^j(\vec{r}) = -A_j p_{O_2}^2 I(\vec{r}). \tag{8}$$

Having compared equations (1) and (7) it can be easily verified that

$$\frac{g(R)}{p_{O_2}} = (p_{O_2}R)\sum_j A_j e^{-\lambda_j p_{O_2} R}. \tag{9}$$

The solution of the problem requires fitting of the function $g(R)/p_{O_2}$ by series of exponents multiplied by $(p_{O_2}R)$. After the fitting, the photoionization problem can be solved by solving differential equations (8) and performing summation

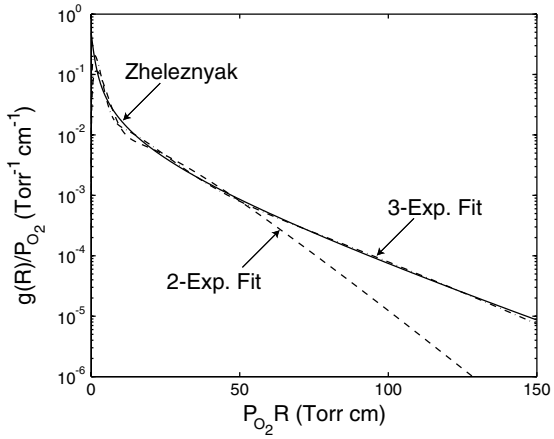

Figure 2. Solid line: The $g(R)/p_{O_2}$ function given by equation (3) from the model of Zheleznyak *et al* (1982). Dashed line: two-exponential fit of the form specified by equation (9), performed for the range $1 < p_{O_2}R < 60$ Torr cm and with the parameters of table 1. Dot-dashed line: three-exponential fit with the parameters of table 2 performed for the range $1 < p_{O_2}R < 150$ Torr cm.

Table 1. Parameters of the two-exponential fit of $g(R)/p_{O_2}/(p_{O_2}R)$ as a function $p_{O_2}R$.

j	A_j (cm^{-2} Torr^{-2})	λ_j (cm^{-1} Torr^{-1})
1	0.0021	0.0974
2	0.1775	0.5877

(6). In practice, it appears to be easier to fit the function $g(R)/p_{O_2}/(p_{O_2}R)$ with a sum of exponents $\sum_j A_j e^{-\lambda_j p_{O_2} R}$ and then multiply the result by $(p_{O_2}R)$ to obtain the desired representation of $g(R)/p_{O_2}$ given by (9).

The function $g(R)/p_{O_2}$ is shown in figure 2 by the solid line and a two-exponential fit performed by MATLAB function fminsearch (based on the Nelder–Mead simplex direct search method) is shown by the dashed line. The two-exponential fit was performed for the range $1 < p_{O_2}R < 60$ Torr cm, which directly corresponds to the $p_{O_2}R$ range shown in figure 3 of Zheleznyak *et al* (1982). The two-exponential fit parameters are shown in table 1. We emphasize that the fit shown in figure 2 by the dashed line is a product of $(p_{O_2}R)$ and $\sum_j A_j e^{-\lambda_j p_{O_2} R}$ as required for solution of the problem and represented by the right-hand side in equation (9). It is also noted that it is very difficult to fit the $g(R)/p_{O_2}$ function with two exponents multiplied by $p_{O_2}R$ and the fit given by parameters in table 1 and in figure 2 becomes invalid for $p_{O_2}R < 1$ Torr cm and $p_{O_2}R > 60$ Torr cm. The implications of this are discussed in section 3.1.

Djakov *et al* (1998) have applied a three-exponential fit in the context of the Zheleznyak *et al* (1982) photoionization model to obtain a fast recursive algorithm for solution of the photoionization problem in a quasi-two-dimensional (the 1.5D or 'disk' based) streamer model. Although the fit proposed in Djakov *et al* (1998) is not directly applicable in the context of the Helmholtz equations based photoionization model discussed in this section, we note that the employment of three-exponential fits represents a natural and logical step to remove the above discussed limitations of the two-exponential model for the range $1 < p_{O_2}R < 60$ Torr cm.

Table 2. Parameters of the three-exponential fit of $g(R)/p_{O_2}/(p_{O_2}R)$ as a function $p_{O_2}R$.

j	A_j (cm^{-2} Torr^{-2})	λ_j (cm^{-1} Torr^{-1})
1	1.986×10^{-4}	0.0553
2	0.0051	0.1460
3	0.4886	0.89

As part of this work we also performed a three-exponential fit of $g(R)/p_{O_2}$ using three exponents multiplied by $(p_{O_2}R)$. The related fit is shown in figure 2 by the dot-dashed line. The parameters of the three-exponential fit are summarized in table 2. The three-exponential fit is valid in the range of $p_{O_2}R$ from 1 to 150 Torr cm. We note that this range translates into $1/150 = 0.0067$ to 1 cm at ground pressure. The fit for $p_{O_2}R > 1$ Torr cm is generally improved in comparison with the two-exponential case, but it is very difficult to fit this function even with three exponents at $p_{O_2}R < 1$ Torr cm. We note that the upper limit of validity of the developed three-exponential fit ($p_{O_2}R = 150$ Torr cm) exceeds the $p_{O_2}R \simeq 100$ Torr cm (i.e. $pR \simeq 500$ Torr cm, where p is air pressure) validity threshold of the Zheleznyak *et al* (1982) model for photoionization in air, as discussed recently in Naidis (2006).

The accurate numerical solution of Helmholtz equations (8) requires knowledge about values of $S^j_{ph}(\vec{r})$ functions at the boundaries of the simulation domain. In Luque *et al* (2007) these values are assumed to be zero. In section 3.1 we demonstrate that the definition of the boundary conditions for different components $S^j_{ph}(\vec{r})$ represents an important part of an accurate solution of the photoionization problem. A practical solution of this problem, which is extensively demonstrated in section 3.1, involves definition of the boundary conditions for $S^j_{ph}(\vec{r})$ component with the smallest λ_j (i.e. the longest photoionization range) using the classic integral model of Zheleznyak *et al* (1982), and assumption of zero boundary conditions for the rest of the $S^j_{ph}(\vec{r})$ components. For both two and three-exponential models presented in this section the smallest λ_j are associated with the first terms in the corresponding series (i.e. with the $j = 1$ term), as can be directly seen from tables 1 and 2. It is expected that this approach may lead to inaccurate results for situations when the photoionization source is positioned very close to the boundary (i.e. for a streamer head approaching an electrode or a dust particle (Babaeva *et al* 2006)). The enhancement of the electric field due to the conducting surface (i.e. image) effects in this kind of simulation geometry may result in a relatively small contribution of the photoionization rate in comparison with the electron-ion pair production rate due to the direct electron impact ionization. Nevertheless, this type of simulation scenarios should be carefully tested with the integral photoionization model (Zheleznyak *et al* 1982) before two and three-exponential Helmholtz models and the Eddington and SP_3 models discussed in the following section, which also rely on the above discussed boundary conditions, can be reliably applied.

2.3. Three-group Eddington and SP_3 approximations for photoionization in air

In Ségur *et al* (2006), the photoionization source term $S_{ph}(\vec{r})$ is calculated using direct numerical solutions of the first

(we also refer to it as Eddington approximation in this paper) and the third order (we also refer to it as SP_3 in this paper following Ségur *et al* (2006)) Eddington approximations of the radiative transfer equation. Ségur *et al* (2006) introduce a simple monochromatic approach (we also refer to it as one-group method in this paper following Ségur *et al* (2006)) and derive the physical parameters required for applying this method to calculating $S_{\rm ph}(\vec{r})$ for non-thermal gas discharges in air at atmospheric pressure by making the model results as consistent as possible with the classical Zheleznyak model.

In order to achieve a better agreement with the Zheleznyak model for the Eddington and SP_3 approximations, we propose to consider $j = 1, N_g$ effective monochromatic radiative transfer equations. For each frequency, the effective monochromatic radiative transfer equation can be written as (Ségur *et al* 2006):

$$\vec{\Omega} \cdot \vec{\nabla} \Psi_j(\vec{r}, \vec{\Omega}) + \lambda_j p_{O_2} \Psi_j(\vec{r}, \vec{\Omega}) = \frac{n_u(\vec{r})}{4\pi c \tau_u}, \qquad (10)$$

where the time dependence of the equation is dropped for convenience in this paper, $\lambda_j p_{O_2}$ is the absorption coefficient and only one excited state u is considered in order to simplify notations. It is important to mention that all monochromatic equations for $j = 1, N_g$ have the same source term but different absorption coefficients. Equation (10) can be simply integrated to derive $\Psi_{0,j}(\vec{r})$, the isotropic part of the photon distribution function $\Psi_j(\vec{r}, \vec{\Omega})$ as

$$\Psi_{0,j}(\vec{r}) = \iiint_{V'} \frac{n_u(\vec{r'})}{c\tau_u} \frac{\exp(-\lambda_j p_{O_2} R)}{4\pi R^2} \, dV'. \qquad (11)$$

Then we assume that the isotropic part of the total distribution function $\Psi_0(\vec{r})$ can be written as

$$\Psi_0(\vec{r}) = \sum_j \alpha_j \Psi_{0,j}(\vec{r}), \qquad (12)$$

where α_j are constants. This approach is similar to the Gaussian-type quadratures generally used in the correlated-k method (Taine and Soufiani 1999). As already mentioned in Ségur *et al* (2006), to calculate the photoionization source term it is only necessary to know $\Psi_0(\vec{r})$, the isotropic part of the distribution function. Then, using equations (11) and (12), the photoionization source term can be written as

$$S_{\rm ph}(\vec{r}) = \sum_j A_j \xi p_{O_2} \iiint_{V'} \frac{n_u(\vec{r'})}{\tau_u} \frac{\exp(-\lambda_j p_{O_2} R)}{4\pi R^2} dV'$$
$$= \sum_j S_{{\rm ph},j}(\vec{r}) \qquad (13)$$

where $A_j \xi p_{O_2}$ are coefficients, which are defined below, with the photoionization efficiency ξ introduced in equation (2). To use this approach in air, the photoionization source term given by equation (13) has to be compared with the Zheleznyak integral expression (1). Both equations are identical if

$$\frac{g(R)}{p_{O_2}} = \sum_j A_j e^{-\lambda_j p_{O_2} R}, \qquad (14)$$

where A_j and λ_j are the unknowns. To obtain their values, we follow the idea in section 2.2 to fit the function $g(R)/p_{O_2}$ by a three-exponential fit (i.e. $N_g = 3$). The corresponding parameters A_j and λ_j are given in table 3. In the following, this approach is called the three-group method.

Table 3. Parameters of the three-exponential fit of $g(R)/p_{O_2}$ as a function $p_{O_2}R$

j	A_j ($\rm cm^{-1}\,Torr^{-1}$)	λ_j ($\rm cm^{-1}\,Torr^{-1}$)
1	0.0067	0.0447
2	0.0346	0.1121
3	0.3059	0.5994

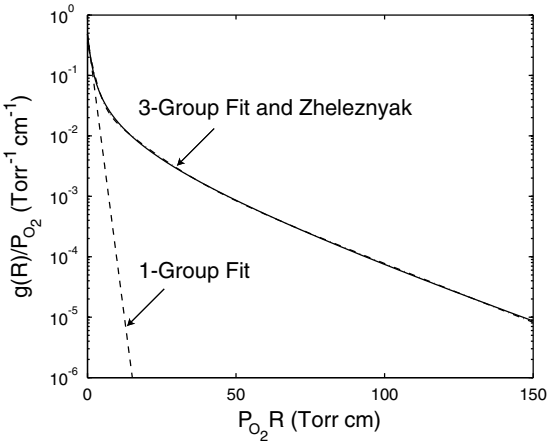

Figure 3. Solid line: The $g(R)/p_{O_2}$ function given by equation (3) from the model of Zheleznyak *et al* (1982). Dashed line: one-exponential fit given in Ségur *et al* (2006). Dot-dashed line: three-exponential fit of the form specified by equation (14), performed for the range $0.1 < p_{O_2}R < 150$ Torr cm, and with the parameters of table 3.

To avoid any possible confusion we emphasize the difference between the equation (14) and the equation (9) of the Helmholtz model. The Helmholtz model employs series of exponents multiplied by $(p_{O_2}R)$, while equation (14) provides direct fit by exponents without multiplication by $(p_{O_2}R)$. We also bring to the attention of the readers the related difference in units between A_j coefficients shown in tables 1 and 2 for the Helmholtz model ($\rm cm^{-2}\,Torr^{-2}$) and those corresponding to equation (14) and shown in table 3 ($\rm cm^{-1}\,Torr^{-1}$).

Figure 3 shows the original function $g(R)/p_{O_2}$, the three-exponential fit (14) derived in this section and the one-exponential fit proposed in Ségur *et al* (2006). The three-exponential fit was performed for the range $0.1 < p_{O_2}R < 150$ Torr cm. It appears that the three-exponential fit allows to have an excellent agreement with the function $g(R)/p_{O_2}$, which is much better than the one-exponential fit, in particular for large $p_{O_2}R$ values. It is interesting to note that in the $p_{O_2}R$ range $0.1 < p_{O_2}R < 150$ Torr cm the fit obtained using a three-group method (figure 3) is generally more accurate than the one obtained using a three-exponential Helmholtz model (figure 2).

The above analysis indicates that in order to calculate the photoionization source term $S_{\rm ph}(\vec{r})$, the set of radiative transfer equations (10) has to be solved. Different methods can be used. In this work we extend to the three-group approach the Eddington and SP_3 methods used in Ségur *et al* (2006) for a one-group approach. For $j = 1, N_g$, the Eddington approximation of (10) to derive $\Psi_{0,j}$ is given by

Ségur *et al* (2006):

$$[\nabla^2 - 3(\lambda_j p_{O_2})^2]\Psi_{ED,0,j}(\vec{r}) = -3\lambda_j p_{O_2}\frac{n_u(\vec{r})}{c\tau_u}, \quad (15)$$

where $\Psi_{ED,0,j}(\vec{r})$ represents the first order Eddington approximation of $\Psi_{0,j}(\vec{r})$. As discussed in Ségur *et al* (2006), equation (15) is an elliptic equation, which has a structure very similar to Poisson's equation. Therefore, both Poisson's equation and the Eddington approximation can be solved with the same numerical routine.

Ségur *et al* (2006) also demonstrate that a third order approximation of the radiative transfer equation is more accurate than the Eddington approximation to calculate the photoionization term when the absorption coefficient of the gas is small and the gradient of the source term is large. For j=1, N_g, the SP_3 approximation of $\Psi_{0,j}$ is denoted as $\Psi_{SP_3,0,j}$ and is given by

$$\Psi_{SP_3,0,j}(\vec{r}) = \frac{\gamma_2\phi_{1,j} - \gamma_1\phi_{2,j}}{\gamma_2 - \gamma_1}, \quad (16)$$

where

$$\gamma_n = \tfrac{5}{7}[1 + (-1)^n 3\sqrt{\tfrac{6}{5}}]. \quad (17)$$

The functions $\phi_{1,j}$ and $\phi_{2,j}$ are defined by

$$\nabla^2\phi_{1,j}(\vec{r}) - \frac{(\lambda_j p_{O_2})^2}{\kappa_1^2}\phi_{1,j}(\vec{r}) = -\frac{\lambda_j p_{O_2}}{\kappa_1^2}\frac{n_u(\vec{r})}{c\tau_u}, \quad (18)$$

$$\nabla^2\phi_{2,j}(\vec{r}) - \frac{(\lambda_j p_{O_2})^2}{\kappa_2^2}\phi_{2,j}(\vec{r}) = -\frac{\lambda_j p_{O_2}}{\kappa_2^2}\frac{n_u(\vec{r})}{c\tau_u}, \quad (19)$$

where $\kappa_1^2 = \frac{3}{7} - \frac{2}{7}\sqrt{\frac{6}{5}}$ and $\kappa_2^2 = \frac{3}{7} + \frac{2}{7}\sqrt{\frac{6}{5}}$. It is important to note that unfortunately, there are some misprints in equations (46) and (47) in Ségur *et al* (2006) and these equations should be replaced by (18) and (19).

Equations (18) and (19) again have the same structure as Poisson's equation and can be solved by the same numerical methods.

We note that since equation (15) of the Eddington model and equations (18) and (19) of the SP_3 model are Helmholtz equations of the same structure as equation (8), it is possible to derive related fits to the $g(R)/p_{O_2}$ function of the type specified by equation (9) of the Helmholtz model (see appendix). As demonstrated in the appendix establishment of these mathematical relationships is useful for general evaluation of the performance of the Eddington and SP_3 models.

After obtaining the solution for $\Psi_{ED,0,j}$ or $\Psi_{SP_3,0,j}$, the photoionization source term can be calculated using

$$S_{ph}(\vec{r}) = \sum_j A_j \xi p_{O_2} c\Psi_{0,j}(\vec{r}) \quad (20)$$

by replacing $\Psi_{0,j}$ with $\Psi_{ED,0,j}$ or $\Psi_{SP_3,0,j}$.

The formulation of the above Eddington approximations requires separate evaluations of ξ in equation (20), and $n_u(\vec{r})/\tau_u$ in equation (15) for the first order approximation, or in equations (18) and (19) for the third one. For the Zheleznyak and Helmholtz models, the product $\xi n_u(\vec{r})/\tau_u$ is computed using equation (2) to give the photoionization radiation source utilizing the known term $\xi(\nu_u/\nu_i)$ given by Zheleznyak *et al* (1982). To effectively use the same term in the Eddington approximations, we can slightly change the above formulation by multiplying both sides of equation (15) or equations (18) and (19) by a constant ξ. For example, the following equation is obtained for the first order Eddington approximation:

$$[\nabla^2 - 3(\lambda_j p_{O_2})^2][\xi\Psi_{ED,0,j}(\vec{r})] = -3\lambda_j p_{O_2}\xi\frac{n_u(\vec{r})}{c\tau_u}, \quad (21)$$

where we could define $\Psi^*_{ED,0,j}(\vec{r}) = \xi\Psi_{ED,0,j}(\vec{r})$. This equation is solved for $\Psi^*_{ED,0,j}(\vec{r})$ and, finally, we have

$$S_{ph}(\vec{r}) = \sum_j A_j p_{O_2} c\Psi^*_{ED,0,j}(\vec{r}). \quad (22)$$

By using this formulation, the factor $\xi(n_u(\vec{r},t)/\tau_u)$ in the source term of equation (21) can be directly evaluated by $p_q/(p+p_q)(\xi(\nu_u/\nu_i))\nu_i n_e$ as used by the Zheleznyak and Helmholtz models (see equation (2)).

The same idea can be applied to equations (18) and (19) of the SP_3 model. In this way, it is also demonstrated that we could use different combinations of ξ and ν_u/ν_i as long as their product is consistent with that given by Zheleznyak *et al* (1982).

Similarly to the Helmholtz model discussed in section 2.2, the boundary conditions also play an important role in accurate evaluation of the S_{ph} term using the three-group method discussed in this section. For the three-group models, boundary conditions can be introduced using the same approach as used for the Helmholtz model. For the three-group Eddington model, the boundary condition is set on the $\Psi^*_{ED,0,1}$ function according to equation (22):

$$\Psi^*_{ED,0,1}(\vec{r}) = \frac{S_{ph}(\vec{r})}{p_{O_2}A_1 c}, \quad (23)$$

where $S_{ph}(\vec{r})$ is calculated using the Zheleznyak integral model. We note that following the discussion in section 2.2 we define here boundary conditions for the $\Psi^*_{ED,0,j}$ component with $j = 1$, corresponding to the smallest λ_j value (the longest photoionization range) as apparent from table 3. Zero boundary conditions are assumed for the remaining $\Psi^*_{ED,0,j}$ components corresponding to $j = 2$ and 3. This approach is subject to the same limitations as discussed at the end of section 2.2.

For the three-group SP_3 model, the same boundary condition is set on the functions defined as $\phi^*_{1,1}(\vec{r}) = \xi\phi_{1,1}(\vec{r})$ and $\phi^*_{2,1}(\vec{r}) = \xi\phi_{2,1}(\vec{r})$ according to equations (20) and (16):

$$\phi^*_{1,1}(\vec{r}) = \phi^*_{2,1}(\vec{r}) = \frac{S_{ph}(\vec{r})}{p_{O_2}A_1 c}. \quad (24)$$

For the first order Eddington model, we have also used the classical boundary conditions derived by Marshak (Pomraning 1973, p 55) for various configurations. For example, for the case of a boundary surface with no reflection or emission (i.e. the boundary surface is transparent for the radiative flux emitted in the medium), the value of $\Psi^*_{ED,0,j}$ at the boundary is given by

$$\vec{\nabla}\Psi^*_{ED,0,j}(\vec{r})\cdot\vec{n}_S = -\tfrac{3}{2}\lambda_j p_{O_2}\Psi^*_{ED,0,j}(\vec{r}), \quad (25)$$

where $\vec{n}_S$ is the unit outward boundary surface normal.

It is interesting to note that equations (21) and (25) form a consistent set of closed equations where the unknowns are the $\Psi^*_{\mathrm{ED},0,j}(\vec{r})$ functions. Furthermore, boundary conditions given by equation (25) are very simple to implement and very fast to calculate. One of our objectives in this work is to demonstrate the influence of the boundary conditions on the calculations of the photoionization source term. In sections 3.1 and 3.2 we use the same type of boundary conditions for the Helmholtz and Eddington models based on the accurate definition of the $j = 1$ term from the integral Zheleznyak model. Figure 8 in section 3.1 is the only exception. In figure 8 results obtained with equations (23) and (25) are compared. The optimization of the calculation of boundary conditions will be the subject of a forthcoming paper.

To conclude the discussion in this section we note that to avoid the Eddington or SP_3 approximations, the radiative transfer equation can be solved directly using, for example, the S_N method (Modest 2003, pp 498–530). Although, the cost of this method is in principle higher than that of the Eddington approximation, it is important to note that, as scattering during collisions is ignored in our physical model, no iterations in the S_N method are required, unlike in the Eddington or the improved Eddington approximations. Thus, the S_N method can be competitive with respect to the improved Eddington approximation if, for example, the number of angular directions is limited. This also will be the subject of a future work.

2.4. Streamer equations

In section 3.2 of this paper the three-exponential Helmholtz and the three-group Eddington and SP_3 differential photoionization models formulated in the previous subsections are employed for solution of a realistic double-headed streamer problem. In this section we provide an overview of related equations.

The most common and effective model to study the dynamics of streamers is based on the following convection–diffusion equations for electrons and ions coupled with Poisson's equation (e.g. Kulikovsky 1997):

$$\frac{\partial n_\mathrm{e}}{\partial t} + \vec{\nabla}\cdot n_\mathrm{e}\vec{v}_\mathrm{e} - \vec{\nabla}\cdot(\overline{\overline{D}}_\mathrm{e}\cdot\vec{\nabla}n_\mathrm{e}) = S_\mathrm{ph} + S^+_\mathrm{e} - S^-_\mathrm{e}, \tag{26}$$

$$\frac{\partial n_\mathrm{p}}{\partial t} = S_\mathrm{ph} + S^+_\mathrm{p} - S^-_\mathrm{p}, \tag{27}$$

$$\frac{\partial n_\mathrm{n}}{\partial t} = S^+_\mathrm{n} - S^-_\mathrm{n}, \tag{28}$$

$$\nabla^2 V = -\frac{q_\mathrm{e}}{\epsilon_0}(n_\mathrm{p} - n_\mathrm{n} - n_\mathrm{e}), \tag{29}$$

where subscripts 'e', 'p' and 'n' refer to electrons, positive and negative ions, respectively, n_i is the number density of species i, V is the potential, $\vec{v}_\mathrm{e} = -\mu_\mathrm{e}\vec{E}$ ($\vec{E}$ being the electric field) is the drift velocity of electrons, $\overline{\overline{\mathrm{D}}}_\mathrm{e}$ and μ_e are the diffusion tensor and the absolute value of mobility of electrons, respectively, q_e is the absolute value of electron charge and ϵ_0 is permittivity of free space. On timescales of interest for studies presented in this paper, ions are assumed to be motionless. The S^+ and S^- terms stand for the rates of production and loss of charged particles. The S_ph term is the previously defined rate of electron–ion pair production due to photoionization in a gas volume. In this study the S^+_e and S^+_p production rates have the meaning of the ionization rate due to the electron impact ionization of air molecules, which is denoted as S_i and is discussed in the subsequent sections of this paper in comparison with the photoionization rate S_ph. As already discussed in section 2.1 the S_i rate is defined in a standard fashion as $S_\mathrm{i} = n_\mathrm{e}\nu_\mathrm{i}$ where $\nu_\mathrm{i} = \alpha|v_\mathrm{e}|$ is the ionization frequency and α is the ionization coefficient. This and other coefficients of the model are assumed to be functions of the local reduced electric field E/N, where E is the electric field magnitude and N is the air neutral density. For test studies presented in this paper all transport parameters and reaction rates in air are taken from Morrow and Lowke (1997). In this paper axisymmetric streamers are studied and thus cylindrical coordinates introduced in section 2.1 are used.

We employ two sets of numerical techniques for solving the streamer model equations:

(i) The charged species transport equations are solved using a flux-corrected transport (FCT) method (Ségur *et al* 2006 and references therein). The 3rd order QUICKEST scheme is used as the high order scheme and an upwind scheme for the low order scheme. The flux limiter derived by Zalesak (1979) is adopted for this FCT method. The finite difference form of Poisson's equation is solved using the D03EBF module of the NAG Fortran library (http://www.nag.co.uk).

(ii) The charged species transport equations are solved using a modified Scharfetter–Gummel (SG) algorithm (Kulikovsky 1995), and the finite difference form of Poisson's equation is solved by the successive overrelaxation (SOR) method (see Liu and Pasko 2004 and references cited therein).

We follow the approach discussed in Vitello *et al* (1994) to define the time step for model execution. The time scales of relevance for selection of the time step, which would provide model stability and accuracy, are the Courant δt_c, effective ionization δt_I and dielectric relaxation δt_D time scales, the explicit expressions for which can be found in Vitello *et al* (1994) and which are not repeated here for the sake of brevity. The model time step is calculated as $\delta t = \min(A_\mathrm{c}\delta t_\mathrm{c}, A_\mathrm{I}\delta t_\mathrm{I}, A_\mathrm{D}\delta t_\mathrm{D})$ with $A_\mathrm{c} = 0.5$, $A_\mathrm{I} = 0.05$ and $A_\mathrm{D} = 0.5$. In practical streamer calculations the time step is almost always defined by the minimum value of the ionization time scale corresponding to the maximum field and maximum ionization frequency ν_imax in the streamer head ($\delta t_\mathrm{I} = 1/\nu_\mathrm{imax}$). We note that in our modelling we adopt a small A_I value, which is a factor of two less than that used in Vitello *et al* (1994).

The boundary conditions for the potential required for the solution of Poisson's equation by both techniques outlined above are obtained using integral solutions of Poisson's equation, which account for the known charge distribution inside of the simulation domain (Liu and Pasko 2004). Specifically, we employ the algorithm presented in Babaeva and Naidis (1996) and Liu and Pasko (2004, 2006) to modify boundary conditions for the potential to represent dynamics of double-headed streamers without effects of the electrode image charges. The applied technique allows to use a relatively small simulation domain in transverse (i.e. radial) direction to obtain an accurate solution for the electric potential corresponding to free (i.e. not affected by boundaries) dynamics of streamers in externally applied uniform electric field.

The calculation of the boundary conditions in streamer simulations can be significantly accelerated since only a small number of grids inside of the simulation domain (usually around streamer body and streamer head(s)) possess charge density values significantly contributing to the potential values at the boundary. In practical calculations the simulation domain is scanned to find the maximum magnitude of the charge density value $|\rho_{\max}|$, and it has been verified by separate tests that accounting only for grids with charge density magnitudes, which exceed 0.1% of this value (i.e. $|\rho| > 0.001|\rho_{\max}|$) leads to fast, accurate and robust evaluation of boundary conditions for potential, allowing effective use of simulation domains with very small size in the radial direction. Further improvements in terms of execution speed can be achieved due to a relatively smooth spatial variation of the potential at the boundaries. The potential can be evaluated at a selected set of points and interpolation can be used to obtain the values at all grid points constituting the boundary. Due to a very small time step used in streamer modelling (usually defined by the ionization time scale associated with the large electric field in the streamer head as already mentioned above) it is also possible, especially for preliminary test runs, to evaluate boundary conditions only once during several steps of the model execution. However, for all the streamer results presented in section 3.2 the update of potential boundary conditions has been performed at every time step for maximum accuracy of results.

For photoionization calculations in the streamer model we employ techniques discussed in sections 2.1–2.3 of this paper. Specifically, for this study we have implemented the three-group Eddington and SP_3, the three-exponential Helmholtz and the classical integral models. The quenching pressure is assumed to be $p_q = 30$ Torr, and the ratio $\xi\nu_u/\nu_i$, appearing in (2), is assumed to depend on the reduced electric field as specified in Liu and Pasko (2004). The finite difference forms of the Eddington, SP_3 and Helmholtz photoionization model equations are solved using the same module of the NAG Fortran library used for the solution of Poisson's equation. These three models are implemented within the context of the first set of numerical techniques described above (i.e. the FCT based). Within the context of the second set of numerical techniques (i.e. the SG based), we implemented the classical integral and the Helmholtz models. The finite difference equations of the Helmholtz photoionization model are solved by the SOR method for this case. The modeling results obtained by using different numerical techniques to solve the Helmholtz model equations are very similar and we will not differentiate them in the following sections of this paper.

It is verified by practical tests that very accurate results for the photoionization production rate can be obtained even if the photoionization is calculated once during every ten steps of the execution of the streamer model. This approach is justified due to the very small time step used in the streamer modeling. Additionally, for photoionization calculations the S_{ph} term is usually negligible in the immediate vicinity of the streamer head due to the domination of the ionization term S_i, and electrons created by the photoionization well ahead of the streamer head go through a relatively long (in comparison with the model time step) evolution and avalanche multiplication before they affect the dynamics of the streamer head.

3. Results and discussion

3.1. Gaussian photoionization source

In this section, a simple model source of photoionizing radiation is used to compare the two and three-exponential Helmholtz, the three-group Eddington and SP_3 models introduced in previous sections 2.2 and 2.3 with the integral model proposed by Zheleznyak *et al* (1982) reviewed in section 2.1. We calculate the photoionization production rate S_{ph} in a two-dimensional axisymmetric computational domain of length L_d and radius R_d for a Gaussian source centered on the symmetry axis. The Gaussian ionization production rate S_i is defined by

$$S_i(r_s, z_s) = \nu_i(r_s, z_s)n_e(r_s, z_s) = S_{i0}\exp(-(z_s - z_0)^2/\sigma^2 - r_s^2/\sigma^2), \quad (30)$$

where z_0 is the axial position of the source term, σ is the parameter controlling effective spatial width of the source, and $S_{i0} = 1.53 \times 10^{25}\,\mathrm{cm^{-3}\,s^{-1}}$. We note that the particular S_{i0} value is chosen to be consistent with similar study presented in Ségur *et al* (2006) and has no implications for test results and related conclusions presented in this section. Assuming $p_q/(p + p_q) = 0.038$ (i.e. ground pressure) and $\xi\nu_u/\nu_i = 0.06$ as in Ségur *et al* (2006) and using (2) we can write

$$I(r_s, z_s) = I_0\exp(-(z_s - z_0)^2/\sigma^2 - r_s^2/\sigma^2), \quad (31)$$

where $I_0 = S_{i0}\xi(\nu_u/\nu_i)p_q/(p + p_q) = 3.5 \times 10^{22}\,\mathrm{cm^{-3}\,s^{-1}}$ as in Ségur *et al* (2006).

The finite difference forms of the differential equations involved in the Helmholtz, Eddington and SP_3 models are solved using the module D03EBF of the NAG Fortran library (http://www.nag.co.uk). The numerical calculation of (4) was carried out using the standard Gaussian quadratures. All calculations were carried out with a uniform grid in both directions and with $n_z = n_r = 251$, where n_z and n_r are the number of cells along the longitudinal and radial directions, respectively.

To demonstrate the importance of different ranges of $p_{O_2}R$ in the solution of the photoionization problems we have performed calculations for simulation domain sizes (i.e. $L_d \times R_d$) $0.02 \times 0.02\,\mathrm{cm^2}$, $0.2 \times 0.2\,\mathrm{cm^2}$ and $2 \times 2\,\mathrm{cm^2}$, at ground pressure ($p_{O_2} = 150$ Torr). We have also used the respective values of source sizes $\sigma = 0.001$, 0.01 and 0.1 cm. It is assumed that the source is positioned in the centre of the simulation domain at $z_0 = 0.01$ cm, 0.1 cm and 1 cm, respectively. It is noted that $\sigma = 0.001$ cm is generally smaller than the dimension of streamer head at ground pressure after it has just been born from an avalanche. The $\sigma = 0.01$ cm is comparable to the size of the streamer head. The streamer head can reach dimension comparable to and much greater than $\sigma = 0.1$ cm in large applied electric field, when the streamer expands quickly (e.g. Briels *et al* 2006, Liu and Pasko 2004). Therefore, all source sizes σ studied in this subsection can be attributed to practical stages of propagation of real streamers.

We note that the artificial source of photoionizing radiation formulated for studies in this section is spherically symmetric and is expected to produce identical distributions of the photoionization production rate S_{ph} in both the radial and the axial directions with respect to the center of the simulation

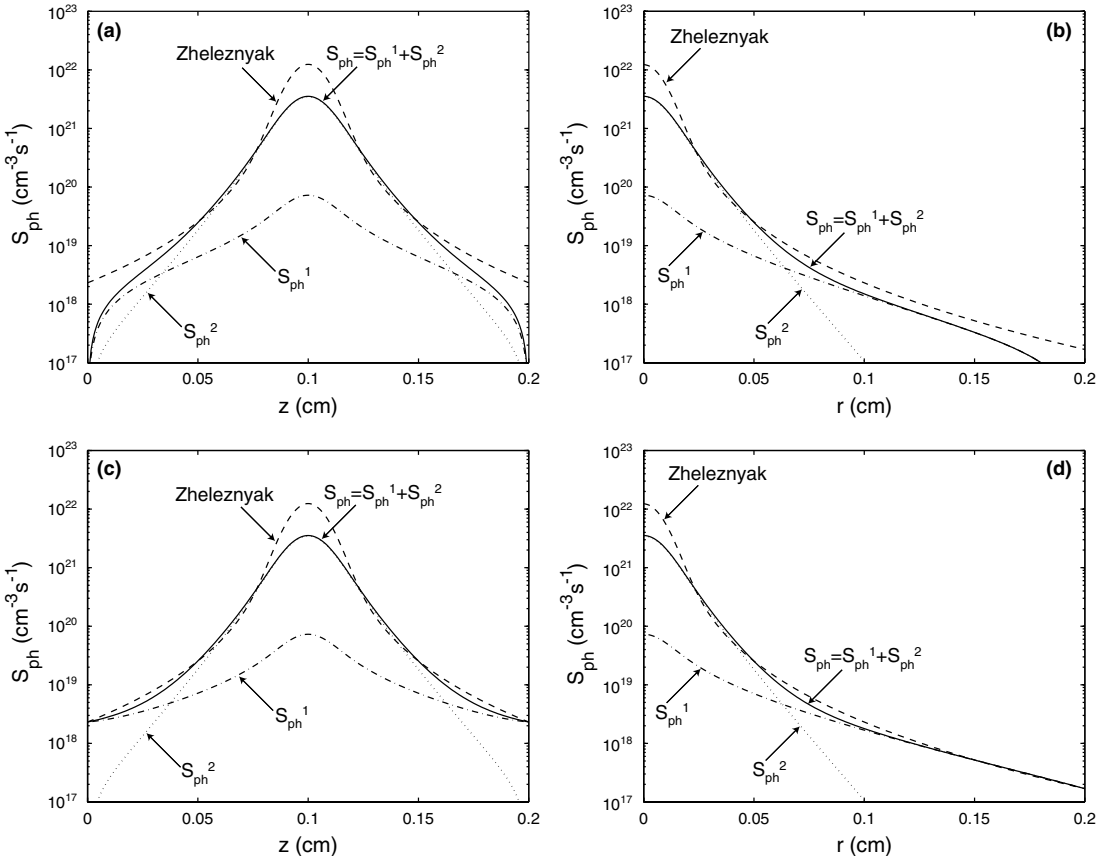

Figure 4. Axial ((*a*) and (*c*)) and radial ((*b*) and (*d*)) profiles of the photoionization source term S_{ph} for the case of domain dimension $0.2 \times 0.2\,\mathrm{cm}^2$ and $\sigma = 0.01\,\mathrm{cm}$. Dashed line: results obtained with integral model of Zheleznyak *et al* (1982). Solid line: the photoionization source term $S_{ph} = S^1_{ph} + S^2_{ph}$ calculated using the two-exponential Helmholtz model with zero boundary conditions ((*a*) and (*b*)), and with corrected boundary conditions ((*c*) and (*d*)). Dot–dashed line: the S^1_{ph} component. Dotted line: the S^2_{ph} component.

domain. Therefore for the chosen domain sizes with $L_d = R_d$, the distance from the center to the radial boundary is two times longer than to the axial boundary. This aspect is very useful for demonstration of effects of boundaries and boundary conditions on obtained solutions as well as for direct comparison of performance of the models on different spatial scales.

Figures 4(*a*) and (*b*) show the axial and radial profiles of the photoionization source term S_{ph} calculated by the Zheleznyak integral model and the Helmholtz differential model based on the two-exponential fit, for the domain dimension $0.2 \times 0.2\,\mathrm{cm}^2$. The two components S^1_{ph} and S^2_{ph} of the two-exponential Helmholtz model are also shown. The solutions of the Helmholtz equations are obtained using zero boundary conditions. We note that the two-exponential Helmholtz profiles deviate significantly from the Zheleznyak solution, especially near the boundaries. The importance of the boundaries in the context of the differential equation based photoionization models has not been discussed in Ségur *et al* (2006) and Luque *et al* (2007).

As already mentioned in section 2.2, the Zheleznyak integral model can be used to improve the solution of the Helmholtz model. Using (4), the boundary condition is defined for the S^1_{ph} component (i.e. for the one with the smallest λ_j). For the other component S^2_{ph}, zero boundary conditions are used. Figures 4(*c*) and (*d*) show axial and radial profiles for the two-exponential model with thus corrected boundary conditions. The solutions are obviously improved.

The effects of the boundary conditions are also very similar to those presented in figure 4 for the Eddington and SP_3 models (related results are not shown here for the sake of brevity). Therefore, in the remainder of this section and in the following section 3.2 all Helmholtz, Eddington and SP_3 model results are obtained using the corrected boundary conditions. Figures 8 and 13 represent two exceptions. Figure 8 shows the influence of the choice of boundary conditions for the Eddington approach, and figure 13 explicitly demonstrates the effects of boundary conditions in the context of practical streamer simulations.

Figures 5(*a*) and (*b*) compare the two and three-exponential Helmholtz model solutions, for the domain dimension $0.2 \times 0.2\,\mathrm{cm}^2$. The ionization term S_i (30) is also included for reference, as for streamer simulations, photoionization is important only in regions where $S_i < S_{ph}$. The results obtained with the three-exponential fit appear to match better with the Zheleznyak integral solution. In particular, the solutions near the center of the simulation domain are significantly improved. This directly relates to a better three-exponential fit at small $p_{O_2} R$ values as can be seen in figure 2.

Figures 5(*c*) and (*d*) compare the Zheleznyak model with results obtained using the 3-group Eddington approximation

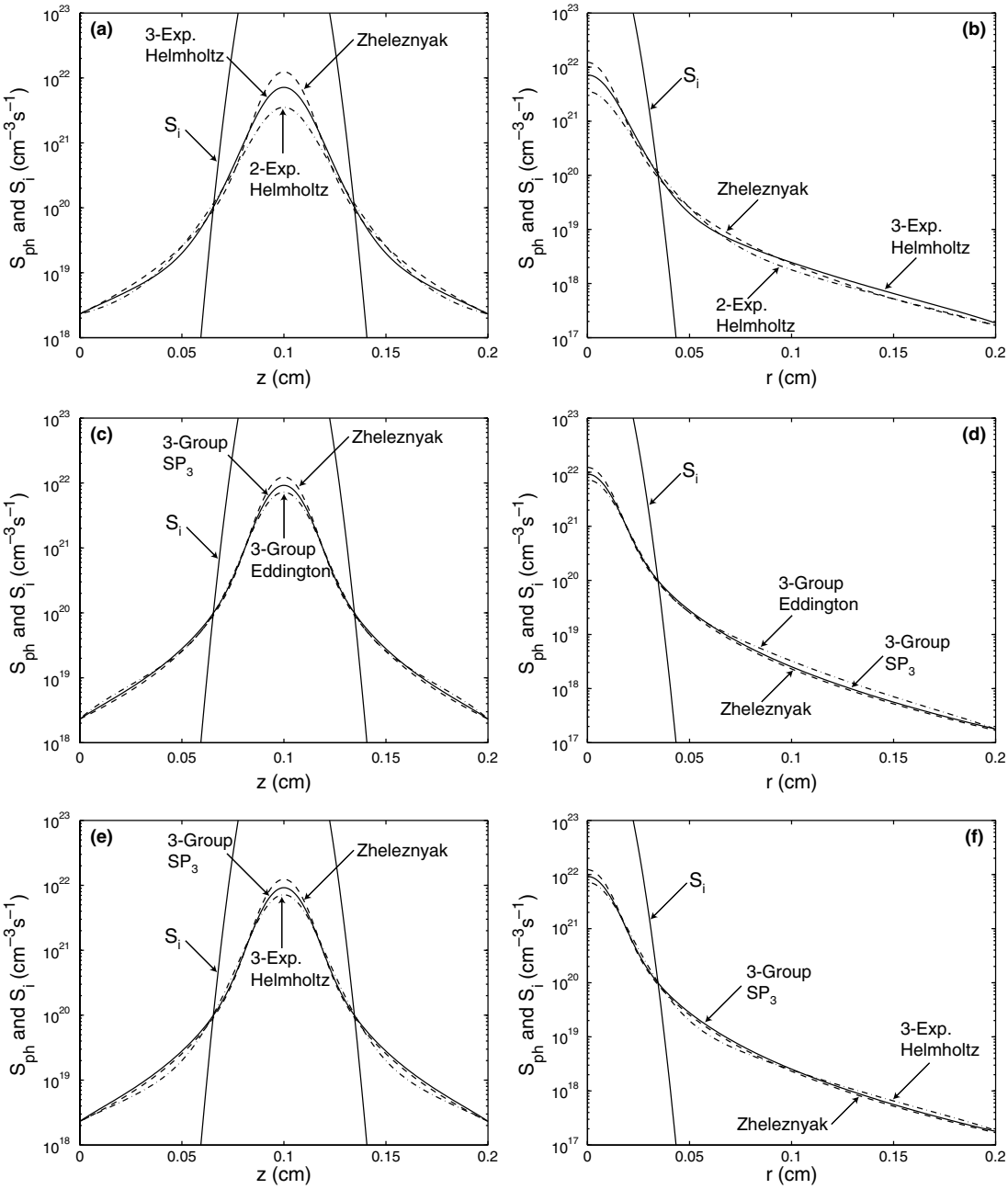

Figure 5. Axial ((*a*), (*c*) and (*e*)) and radial ((*b*), (*d*) and (*f*)) profiles of the ionization source term S_i and the photoionization source term S_{ph}, for the case of domain dimension $0.2 \times 0.2\,\mathrm{cm}^2$ and $\sigma = 0.01\,\mathrm{cm}$. Dashed line: results obtained with integral model of Zheleznyak *et al* (1982). (*a*) and (*b*) dot-dashed line: S_{ph} using the two-exponential Helmholtz model, Solid line: S_{ph} using three-exponential Helmholtz model. (*c*) and (*d*) dot-dashed line: S_{ph} using 3-group Eddington approximation, solid line: S_{ph} using 3-group SP_3. (*e*) and (*f*) solid line: S_{ph} using 3-group SP_3 approximation, dot-dashed line: S_{ph} using 3-exponential Helmholtz model.

and the 3-group SP_3 model, for the same domain dimension $0.2 \times 0.2\,\mathrm{cm}^2$. The results shown in these two figures demonstrate that the 3-group Eddington approximation and the 3-group SP_3 model give very similar results in the region where $S_{ph} > S_i$, and these two solutions also appear to be in good agreement with the Zheleznyak integral model. At atmospheric pressure ($p_{O_2} = 150\,\mathrm{Torr}$), the three absorption coefficients of the three-group Eddington and SP_3 models given in table 3 are $\lambda_1 p_{O_2} = 6\,\mathrm{cm}^{-1}$, $\lambda_2 p_{O_2} = 16\,\mathrm{cm}^{-1}$ and $\lambda_3 p_{O_2} = 89\,\mathrm{cm}^{-1}$. It is interesting to note that even if the Eddington and SP_3 are in principle only very well suited to situations in which photon absorption is sufficiently high (Ségur *et al* 2006), figure 5 shows that these approximations can be used to calculate accurately the photoionization source term using a three-group approach for streamer propagation.

Finally, in figures 5(*e*) and (*f*), we compare the 3-group SP_3 and the 3-exponential Helmholtz model with the Zheleznyak model. The SP_3 model appears to be slightly more accurate in the region where $S_{ph} > S_i$.

We note that the direct application to the streamer modelling of the Zheleznyak integral model given by equation (1), without optimizations specified in section 2.1, is

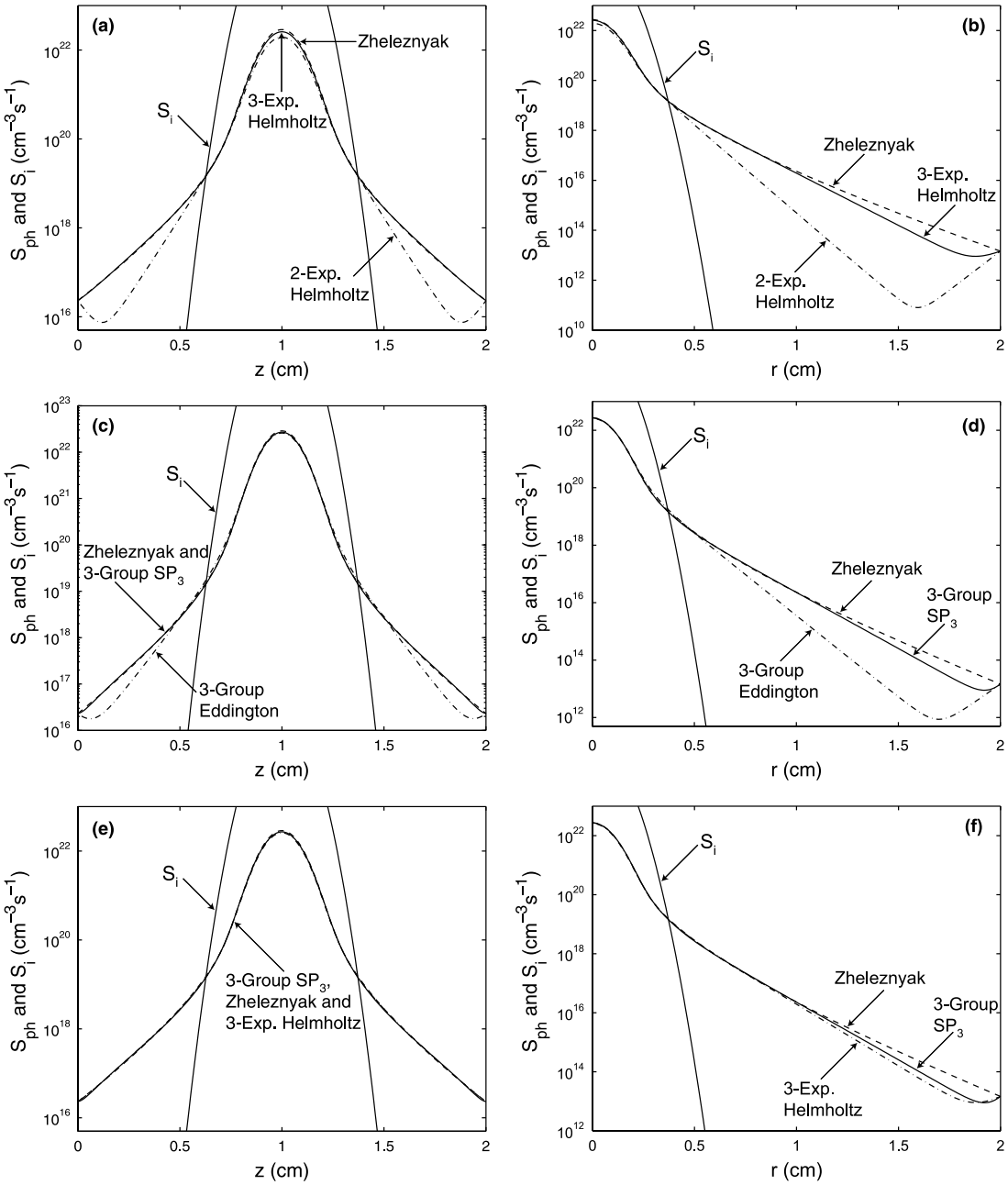

Figure 6. Same caption as figure 5 only for domain dimension $2 \times 2\,\mathrm{cm}^2$ and $\sigma = 0.1\,\mathrm{cm}$.

prohibitively computationally expensive. In particular, results obtained in figure 5 using the non-optimized Zheleznyak model generally required a factor of 1000 longer computational times than those obtained with the Eddington and Helmholtz models.

Figure 6 presents the same information as figure 5, only for the domain dimension $2 \times 2\,\mathrm{cm}^2$ with $\sigma = 0.1\,\mathrm{cm}$.

Figures 6(*a*) and (*b*) show the axial and radial profiles of the photoionization source term S_{ph} calculated by the Zheleznyak model in comparison with the Helmholtz solutions obtained using the two and three-exponential fits. As in figure 5, the ionization term S_{i} is also shown for reference. The results obtained with the three-exponential fit appear to match better with the Zheleznyak integral solution in the region where $S_{\mathrm{ph}} > S_{\mathrm{i}}$ and, in particular, close to the boundaries. The two-exponential Helmholtz model fails to provide an accurate solution in this case. This result directly relates to a poor two-exponential fit at large $p_{\mathrm{O}_2} R > 60\,\mathrm{Torr\,cm}$ values (i.e. $R > 0.5\,\mathrm{cm}$ at ground pressure considered here), as can be seen in figure 2. The better performance of the three-exponential Helmholtz model directly relates to a better three-exponential fit at large $p_{\mathrm{O}_2} R$ values (i.e. $R > 0.5\,\mathrm{cm}$ at ground pressure), as can also be seen in figure 2.

Figures 6(*c*) and (*d*) compare the 3-group Eddington approximation and the 3-group SP_3 with the Zheleznyak model for the same domain dimension $2 \times 2\,\mathrm{cm}^2$. We note that the use of the SP_3 allows to improve the agreement with the Zheleznyak model, in particular, close to the boundaries.

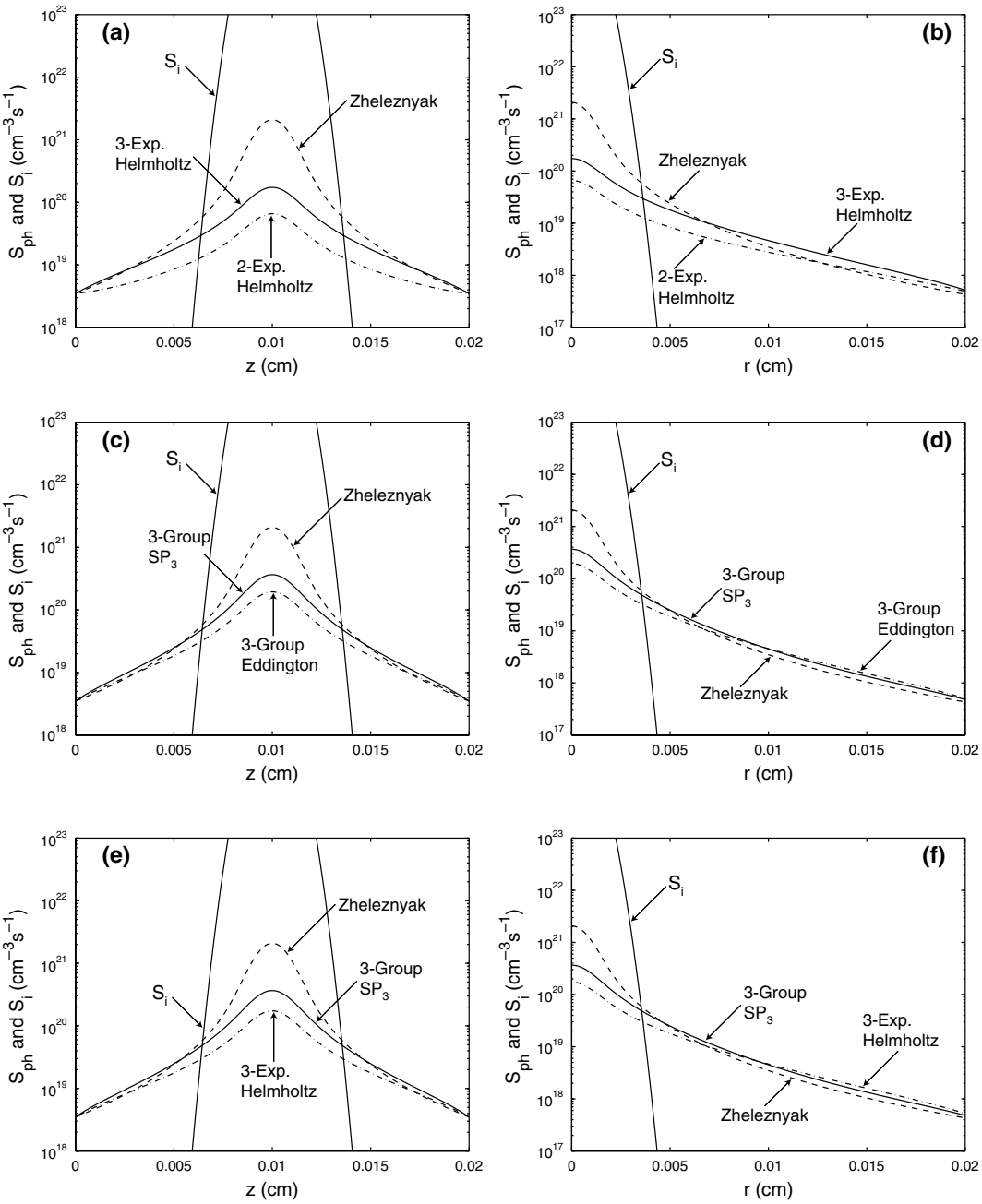

Figure 7. Same caption as figure 5 only for domain dimension $0.02 \times 0.02\,\mathrm{cm}^2$ and $\sigma = 0.001$ cm.

Finally, figures 6(*e*) and (*f*) compare the 3-group SP_3 and the 3-exponential Helmholtz model with the Zheleznyak model. In this case, both models give very similar results in the axial direction and are very close to the Zheleznyak model. In the radial direction, the results obtained with the SP_3 model appear to be slightly more accurate than the three-exponential Helmholtz model in the region where $S_{ph} > S_i$.

As we emphasized at the beginning of this section, for the domain with $L_d = R_d$ the effective distance from the source at the center of the simulation domain to the boundary is two times longer in the radial direction than in the axial direction (i.e. 2 cm versus 1 cm in figure 6). Therefore the radial distances exceeding 1 cm allow one to observe the behavior of different models in the region beyond applicability of the model fits obtained for the range $1 < p_{O_2}R < 150$ Torr cm for the three-exponential Helmholtz model (figure 2) and for $0.1 < p_{O_2}R < 150$ Torr cm for the three-group Eddington and SP_3 models (figure 3) (i.e. for $R < 1$ cm at atmospheric pressure $p_{O_2} = 150$ Torr). All models shown in figures 6(*e*) and (*f*) show outstanding performance in both axial and radial directions at distances <1 cm from the source, as expected from the range of validity of related fits in figures 2 and 3. In the same vein we note that a special caution should be used when models described in this work are applied in large simulation domains for which $p_{O_2}R$ product exceeds 150 Torr cm.

Figure 7 is presented in the same format as figures 5 and 6, only for the domain dimension $0.02 \times 0.02\,\mathrm{cm}^2$ with $\sigma = 0.001$ cm.

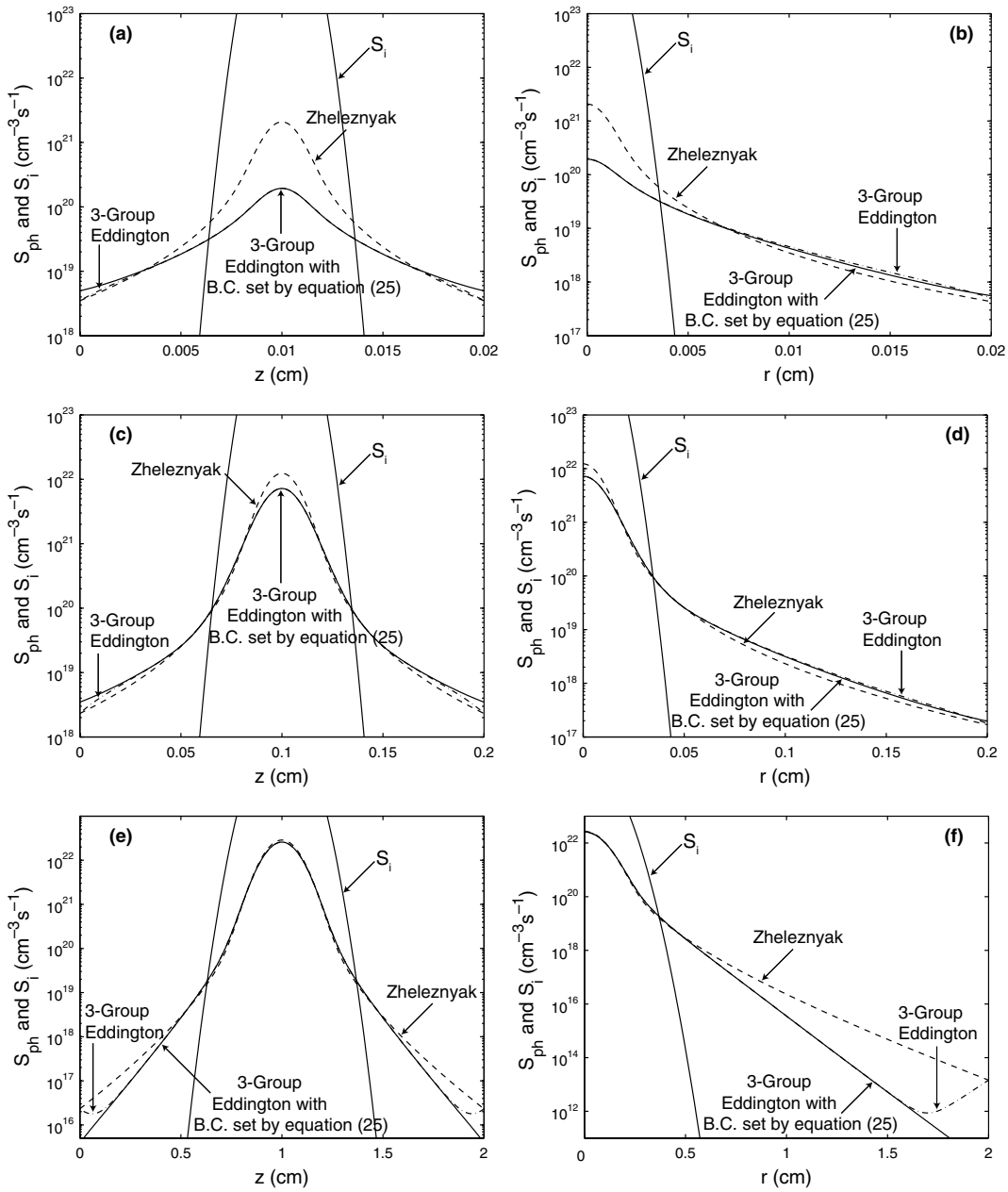

Figure 8. Axial ((*a*), (*c*) and (*e*)) and radial ((*b*), (*d*) and (*f*)) profiles of the ionization source term S_i and the photoionization source term S_{ph}. Dashed line: S_{ph} using the integral model of Zheleznyak *et al* (1982). Solid line: S_{ph} using 3-group Eddington approximation and boundary conditions given by equation (25), dot-dashed line: S_{ph} using 3-group Eddington model with boundary conditions given by equation (23), (*a*) and (*b*) for the case of domain dimension $0.02 \times 0.02\,\mathrm{cm}^2$ and $\sigma = 0.001$ cm; (*c*) and (*d*) for the case of domain dimension $0.2 \times 0.2\,\mathrm{cm}^2$ and $\sigma = 0.01$ cm, (*e*) and (*f*) for the case of domain dimension $2 \times 2\,\mathrm{cm}^2$ and $\sigma = 0.1$ cm.

Figures 7(*a*) and (*b*) show the axial and radial profiles of the photoionization source term S_{ph} calculated by the Zheleznyak model and the Helmholtz solution using two and three-exponential fits. As expected from the fits shown in figure 2 for small distances, the results obtained with both solutions are poor, but we note that in the region of interest for streamer simulations (where $S_{ph} > S_i$), the three-exponential Helmhotz model appears to be in relatively good agreement with the Zheleznyak model.

In figures 7(*c*) and (*d*), we compare the three-group Eddington approximation and the three-group SP_3 with the Zheleznyak model. We note that the use of the SP_3 allows to improve the agreement with the Zheleznyak model, in particular, in the region where $S_{ph} > S_i$.

In figures 7(*e*) and (*f*), we compare the three-group SP_3 and the three-exponential Helmholtz model with the Zheleznyak model. In this case, in the region where $S_{ph} > S_i$ both models give very similar results in the axial direction and are very close to the Zheleznyak model. In the radial direction, the results obtained with the SP_3 model appear to be slightly more accurate than the three-exponential Helmholtz model in the region where $S_{ph} > S_i$.

Finally, figure 8 demonstrates comparative performance of the boundary conditions specified by equations (23) or (25)

for the three-group Eddington approximation. Figures 8(*a*) and (*b*) are for the domain dimension $0.02 \times 0.02\,\mathrm{cm}^2$ with $\sigma = 0.001$ cm, and 8(*c*) and (*d*) are for the domain dimension $0.2 \times 0.2\,\mathrm{cm}^2$ with $\sigma = 0.01$ cm. In both cases, the use of equation (25) slightly overestimates the exact value of the photoionization source term at the boundaries in the axial direction, but the agreement is good in the radial direction. Figures 8(*e*) and (*f*) are for the domain dimension $2 \times 2\,\mathrm{cm}^2$ with $\sigma = 0.1$ cm. In this case, the use of equation (25) underestimates the exact value of the photoionization source term at the boundaries in the axial and radial directions.

We reiterate again the point stated at the end of section 2.3 that equations (21) and (25) form a coherent set of closed equations for the Eddington approach. Furthermore, boundary conditions given by equation (25) are very simple to implement and very fast to calculate.

In conclusion, all the results obtained in this section show that the use of non-zero boundary conditions improves significantly the agreement between the Zheleznyak integral and the approximate differential models. In this work, we have used mainly boundary conditions specified on the basis of the classic integral model of Zheleznyak. In this section we demonstrated that for approximate radiative transfer equations a coherent set of approximate boundary conditions derived from radiation transfer theory can be successfully used. The optimization of the calculation of boundary conditions will be the subject of a future work. We have also shown that the use of a three-exponential fit either with the SP_3 model or with the Helmholtz model allows to obtain a good agreement with the Zheleznyak integral model, and that the two-exponential fit is generally not sufficient to reproduce the Zheleznyak model accurately for the full range of validity of this model (i.e. up to $p_{O_2} R \simeq 100$ Torr cm, or $R \simeq 0.7$ cm at ground pressure (Naidis 2006)). It is interesting to note also that although the Eddington and SP_3 are in principle only very well suited to situations in which photon absorption is sufficiently high, these approximations can be used to calculate accurately the photoionization source term using a three-group approach for streamer propagation. The models derived in this paper are only slightly more complicated than the one-group model proposed in Ségur *et al* (2006), but remain simple to implement in streamer codes. Results of the practical application of these models to a streamer problem are presented in the following section 3.2, in which we also discuss computational expenses involved in different types of photoionization models.

3.2. Double-headed streamers in air

In this section, we report and compare modelling results on a double-headed streamer developing in air at ground pressure (760 Torr) obtained with different photoionization models discussed in previous sections of this paper. The simulation domain is the same as in Liu and Pasko (2004, figure 4(*a*)). Two remote electrodes with a certain potential difference establish a uniform Laplacian field $E_0 = 4.8 \times 10^6\,\mathrm{V\,m^{-1}}$. All results presented in this paper are obtained assuming air neutral density $N_0 = 2.688 \times 10^{25}\,\mathrm{m^{-3}}$, and therefore $E_0/N_0 = 178.6$ Td (1 Td $= 10^{-17}\,\mathrm{V\,cm^2}$). Under the influence of this applied field, a double-headed streamer is launched by placing a neutral plasma cloud in the simulation domain. The initial plasma cloud has a Gaussian distribution in space:

$$n_\mathrm{e}(r,z)|_{t=0} = n_\mathrm{p}(r,z)|_{t=0} = n_0 \exp\left[-\left(\frac{r}{\sigma_r}\right)^2 - \left(\frac{z-z_0}{\sigma_z}\right)^2\right]. \quad (32)$$

The center of the Gaussian distribution is located in the middle of the simulation domain, at $z_0 = 0.7$ cm, and it is assumed that $\sigma_r = \sigma_z = 0.02$ cm and $n_0 = 10^{20}\,\mathrm{m^{-3}}$. The size of the computational domain is $1.4 \times 0.125\,\mathrm{cm}^2$. The computational grid is uniform in both radial and axial directions. The total number of cells is $n_z \times n_r = 1681 \times 151$, where n_z and n_r represent number of cells in the axial and radial directions, respectively. As part of preparatory work for the model studies presented in this paper we have conducted several test runs with 2400×100 grid points with a refined mesh in the radial direction and uniform mesh in the axial direction. Results appeared to be identical to those obtained with the 1681×151 uniform mesh, which therefore was adopted for all runs presented in this paper.

Before the incorporation of different photoionization models, we tested the performance of the two sets of numerical techniques described in section 2.4 (i.e. the FCT and SG based) using a test-case for which photoionization effects are not included and the pre-ionization level is only supplied by a uniform neutral background plasma with initial density of $10^{14}\,\mathrm{m^{-3}}$. This approach is similar to the one applied in a classic paper of Dhali and Williams (1987). Only very small differences are observed in results obtained with the two models for the modelled double-headed streamer. Specifically, by the time moment 3.5 ns from the beginning of the model execution the differences between the peak electron number densities and peak electric fields between two model streamers do not exceed 7.8% and 2.6%, respectively. It is noted that these differences do not exceed those arising from known limitations of the local field approximation in streamer modelling (Naidis 1997, Li *et al* 2007). These test results are not shown in this paper for the sake of brevity, but essentially the same agreement between the two numerical techniques can be observed by comparing results obtained with the three-exponential Helmholtz photoionization model shown in figures 9 and 10(*a*).

Figure 9 compares the electron number density distribution on the symmetry axis of the computational domain calculated using the three-group Eddington and SP_3, and the three-exponential Helmholtz models for the photoionization term. The results are shown for the moments of time from $t = 0$ to $t = 3.5$ ns, with a timestep of 0.5 ns. We note that there is an excellent agreement between the results obtained with these three models for both streamer heads. Small differences are observed in the region well ahead of the streamer head, and the differences increase as the streamer advances.

Figure 10 compares the profiles of electron density and the magnitude of the electric field on the symmetry axis of the computational domain calculated using the three-exponential Helmholtz model for the photoionization term and the classical integral model of Zheleznyak *et al* (1982) optimized as described in section 2.1. The results are also shown for the moments of time from $t = 0$ to $t = 3.5$ ns,

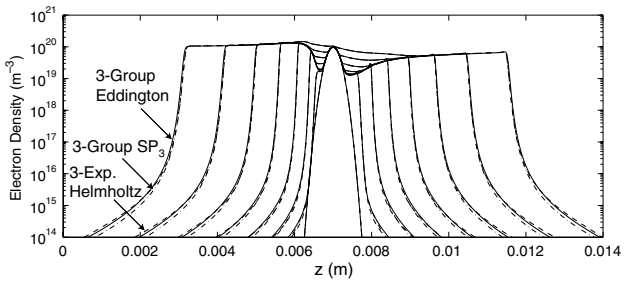

Figure 9. Electron density profiles on the symmetry axis of the computational domain at various moments of time calculated using different photoionization models. The results are obtained by the FCT based numerical technique described in section 2.4. Dashed line: three-exponential Helmholtz model; Solid line: three-group Eddington; Dot-dashed line: three-group SP_3. Results are shown for the moments of time from $t = 0$ to $t = 3.5$ ns, with a timestep of 0.5 ns.

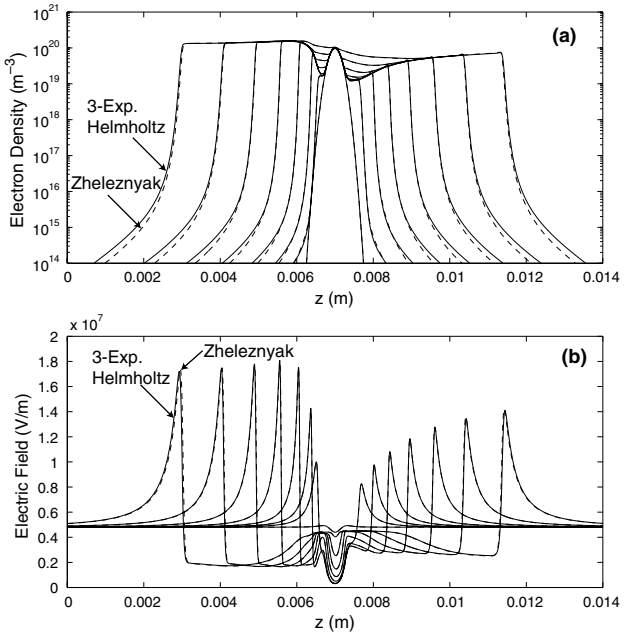

Figure 10. Profiles of streamer characteristics along the symmetry axis of the computational domain at various moments of time calculated using different photoionization models. The results are obtained by the SG based numerical technique described in section 2.4. (*a*) Electron density. (*b*) Electric field. Dashed line: optimized integral Zheleznyak model; Solid line: three-exponential Helmholtz model. Results are shown for the moments of time from $t = 0$ to $t = 3.5$ ns, with a timestep of 0.5 ns.

with a timestep of 0.5 ns. An excellent agreement between the results is observed for the double-headed streamer. For the electron density, only small differences exist in the region well ahead of the streamer head. For electric field, the difference is almost impossible to notice before 3.0 ns and extremely small deviations between results obtained with the two models are present at 3.0 and 3.5 ns. The differences for both electron density and electric field increase as the streamer advances.

Figure 11 shows a cross-sectional view of the distributions of the electron density, electric field and photoionization production rate at $t = 3.5$ ns obtained using the three-exponential Helmholtz model. This cross-sectional view represents an example of two-dimensional views of simulation results obtained by using different differential equation based photoionization models. As expected, the photoionization source term is maximized in the head regions, but we also note that this term is significant in the body of the streamer in the region between the two heads. As expected on physical grounds and as apparent from figure 11(*c*) the photoionization production rate appears to exhibit a high degree of spherical symmetry around both streamer heads. The direct inspection of figure 11(*c*) also emphasizes the importance of accurate definition of boundary conditions for $S_{\rm ph}$, as simple zero boundary conditions on radial boundaries would clearly produce an unphysical distortion of the photoionization production rate.

Figure 12(*a*) shows the $S_{\rm ph}$ term and the relative distributions of the three components of the three-exponential Helmholtz model on the symmetry axis of the simulation domain at $t = 3.0$ ns. The regions dominated by each component can clearly be identified in the figure. The $S^1_{\rm ph}$ term, associated with the smallest λ_1 and therefore with the longest photoionization range (which from the general structure of equation (7) is expected to approximately follow $1/\lambda_1$ dependence) dominates in the region ahead of the streamer head. The $S^2_{\rm ph}$ term ranks after $S^1_{\rm ph}$ demonstrating intermediate λ_2 value and the photoionization range (see table 2), while $S^3_{\rm ph}$ term is clearly confined and dominates inside of the streamer head (this term has the largest λ_3 as can be seen from table 2 and therefore is associated with the shortest photoionization range).

Figure 12(*b*) compares the photoionization source term calculated by the three-exponential Helmholtz model described in section 2.2 and the optimized integral Zheleznyak model described in section 2.1. Results from both models are in very good agreement in the regions of and ahead of both positive (left) and negative (right) streamer heads. A significant difference is observed in the region between the streamer heads. We recall that the optimized integral solution described in section 2.1 does not include contributions from the emission sources outside of the square around each of the streamer heads (see figure 1(*b*), and the discussion at the end of section 2.1), but the Helmholtz solution does. A relatively strong ionization appears in the streamer body (figure 13(*b*)) implying strong photon emission source in this region. The Helmholtz model automatically accounts for this source by the right-hand side term in equation (8). However, the photoionization source in the streamer body does not affect the dynamics of the streamer, because the electron impact ionization rate $S_{\rm i}$ is much stronger than the photoionization rate $S_{\rm ph}$ in the streamer body, as illustrated in figure 13(*b*).

As a follow-up from the discussion presented in the previous paragraph it is worthwhile to reiterate that photoionization plays a role in the streamer dynamics only when it dominates over ionization in certain regions. Figures 13(*a*) and (*b*) compare the photoionization source term $S_{\rm ph}$ calculated with the three-group SP_3 model and the ionization source term $S_{\rm i}$ at two different moments of time: $t = 0.2$ ns and $t = 3$ ns. At $t = 0.2$ ns, we note that in the streamer head regions the ionization term $S_{\rm i}$ exceeds the photoionization term $S_{\rm ph}$. In front of the streamer heads, the photoionization source term dominates. Very rapidly as

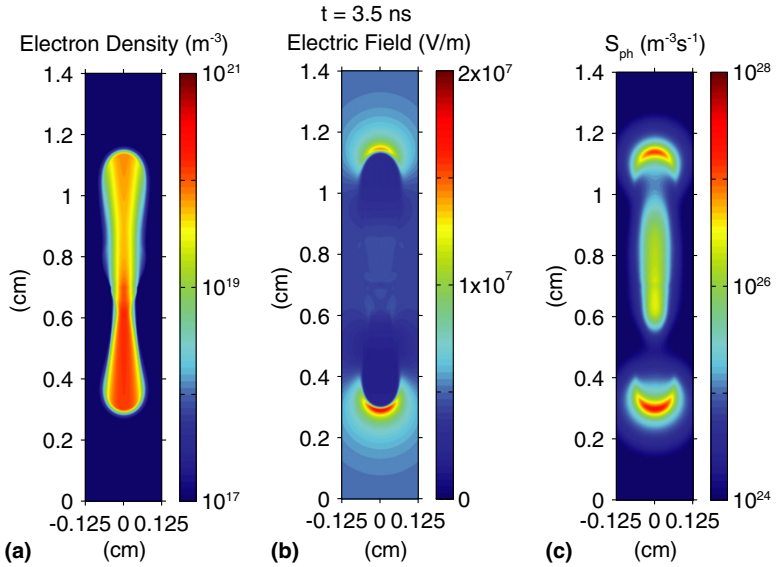

Figure 11. A cross-sectional view of distributions of (*a*) electron density, (*b*) electric field and (*c*) photoionization source term at $t = 3.5$ ns calculated using the three-exponential Helmholtz model.

(This figure is in colour only in the electronic version)

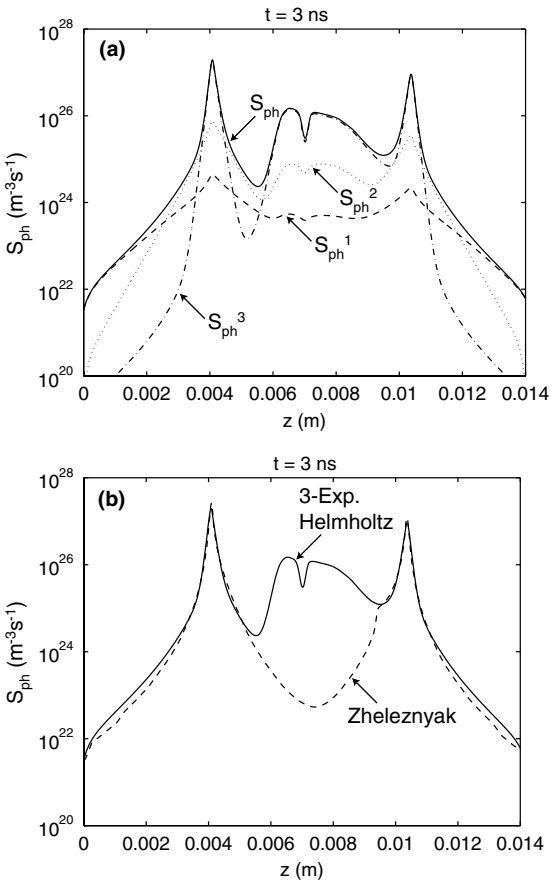

Figure 12. Photoionization source term S_{ph} at $t = 3$ ns along the symmetry axis of the computational domain. (*a*) S_{ph} and the three components S_{ph}^1, S_{ph}^2 and S_{ph}^3 of the three-exponential Helmholtz model. (*b*) S_{ph} calculated using the three-exponential Helmholtz and the optimized integral Zheleznyak models.

the streamer starts to propagate, the ionization term becomes stronger than the photoionization term everywhere in the simulation domain as shown, for example, by figure 13(*b*) at $t = 3$ ns. These results support the conclusion made in Kulikovsky (2000) 'In high field the streamer behaves as a flash lamp; it produces very intensive radiation when it arises and then the initial photoelectrons provide its propagation.' This conclusion is only valid for streamers propagating in a high applied electric field E exceeding the conventional breakdown threshold field E_k defined by the equality of the electron impact ionization and electron dissociative attachment coefficients in air (Raizer 1991, p 135). It is expected that the photoionization term would dominate over the ionization term in most of the region ahead of a streamer propagating in a low ambient field ($E < E_k$) in a point-to-plane discharge geometry where the dissociative and three-body attachment of electrons is dominant over the ionization. The related results in the context of the photoionization models described in this paper will be reported in a separate dedicated publication.

Figures 13(*a*) and (*b*) also show the photoionization source term S_{ph} and the ionization term calculated for a case when zero boundary conditions for the photoionization term S_{ph} in SP_3 model are used. In this case, we note that in the regions of the streamer heads the ionization term dominates over photoionization term; however, the photoionization term is at all moments of time stronger than the ionization term in the region ahead of both streamer heads. This observation reiterates that the boundary conditions for the photoionization calculation have a significant impact on the ionization term as photoionization provides the initial photoelectrons for ionization in high fields. Figures 13(*a*) and (*b*) indicate that in the regions ahead of streamer heads, both photoionization and ionization terms significantly deviate from those calculated using correct boundary conditions for S_{ph}. We emphasize that even with these noticeable differences in ionization and photoionization, the characteristics (e.g. distributions of the electron density and electric field, speed and radius) of the model streamer are

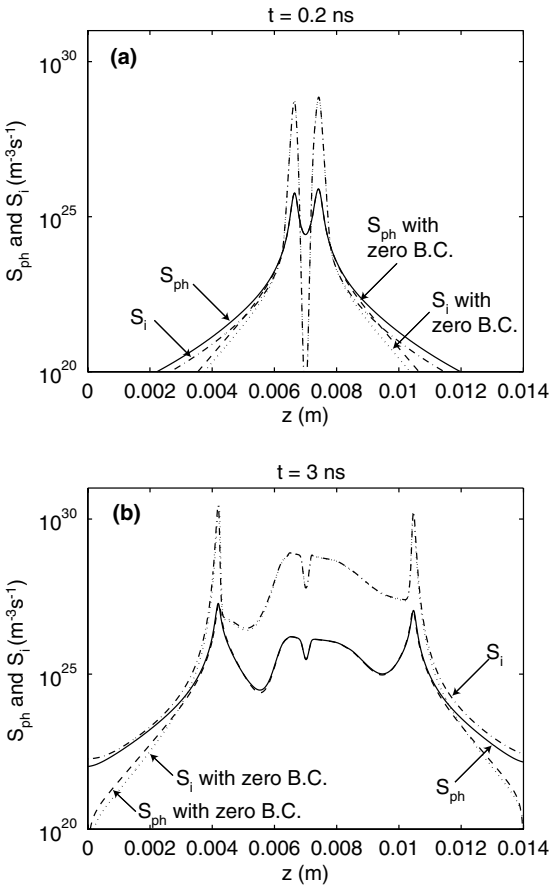

Figure 13. Photoionization source term S_{ph} and ionization source term S_i along the symmetry axis of the computational domain at (*a*) $t = 0.2$ ns and (*b*) $t = 3$ ns. Solid line: the three-group SP_3 with corrected boundary conditions. Dot-dashed line: ionization term with corrected boundary conditions for photoionization. Dashed line: the three-group SP_3 with zero boundary conditions. Dotted line: ionization term with zero boundary conditions for photoionization.

still very close to the case with correct boundary conditions for photoionization. Therefore, for this high field test-case to speed up calculation, it is possible to use zero boundary conditions for photoionization calculation if the goals of the study do not include detailed studies of properties of the ionization or photoionization in the region ahead of the streamer heads. However, as we already mentioned above, for other situations such as the propagation of streamers in low fields in point-to-plane discharge geometry when two and three-body attachment dominates over ionization in the most of the simulation domain ahead of the streamer (i.e. Babaeva and Naidis 1997, Liu and Pasko 2006 and references therein), it is essential to correctly take into account boundary conditions for calculation of the photoionization term, and related studies will be presented in a separate follow up paper.

It is instructive to compare the total execution times of the models based on differential equation approach in comparison with the optimized integral Zheleznyak model. We have noticed that the simulation time of the three-group Eddington approach with boundary conditions given by equation (23) is similar to the one of the three-exponential Helmholtz model with corrected boundary conditions given in section 2.2, whereas the simulation time of the three-group SP_3 with boundary conditions given by equation (24) is slightly longer. As an example of such comparisons we conducted accurate measurements of computation times involved in two model cases shown in figure 10. We reiterate that both models are executed on the same hardware (2 GHz Power Mac G5 running Mac OS X 10.4) with identical grids and algorithms to define time steps and boundary conditions. As already noted in section 2.4 the photoionization production rate has been updated after every ten steps of the model execution and the boundary conditions for the electric potential have been updated every time step. The measured total execution time of the code based on the optimized implementation of the Zheleznyak *et al* (1982) integral photoionization model as described in section 2.1 was 53 h and 20 min. The measured execution time of the code based on the three-exponential Helmholtz model with corrected boundary conditions described in section 2.2 was 63 h and 14 min. The time profiling indicates that about 80% of the model execution time is spent in both cases on updates of the boundary conditions for the potential and the solution of the Poisson equation for the electric field. It is noted that even if the photoionization production rate is updated at every time step, the execution times of both models will be of the same order.

The difference in the computation time presented above may seem in favor to the integral photoionization model; however, it is important to point out that the optimization (introduction of moving meshes with variable cell sizes and employment of effective windowing and interpolation techniques) of the integral model is rather involved and complex, and requires a separate adaptation effort to extend it to every new configuration studied. At the same time, the implementation of the photoionization models based on differential equation approach is straightforward and simple. Furthermore, in the optimized integral approach the photoionization source term is calculated accurately only close to the streamer heads. For example, in the double-headed test-case, we have shown that due to the optimization, in the region between the streamer heads, the photoionization source term is not calculated accurately using the integral model. Conversely with the differential approaches the photoionization term is calculated accurately in the whole computation domain.

4. Conclusions

In this paper, we discuss and improve several models currently proposed in the literature for the calculation of the photoionization produced by plasma discharges in air. The reported improvements are achieved by more accurate accounting for the spectral dependence of the photoionization process. In particular, the classical Zheleznyak integral model and three photoionization models in a differential form are presented. These approaches can be directly applied for photoionization calculations in model studies of the dynamics of streamers in air.

An efficient implementation of the classical Zheleznyak integral model is presented for streamer modeling in air. The three differential approaches developed are a three-exponential Helmholtz model, a three-group Eddington and a three-group

improved Eddington (SP_3) models. The Helmholtz model is based on an approximation of the absorption function of the gas in order to transform the integral expression of the photoionization term in a set of Helmholtz differential equations. The Eddington and SP_3 methods are based on the direct numerical solution of an approximation of the radiative transfer equation. It is demonstrated that the solutions involved in all the three differential models require accurate definition of the boundary conditions.

We have conducted two test studies of the performance of the newly proposed photoionization models: Gaussian emission source and a double-headed streamer developing in a strong uniform electric field (greater than the conventional breakdown field).

Our studies using the Gaussian source have demonstrated that the use of a three-exponential fit to the absorption function in air either with the Eddington, SP_3 or the Helmholtz model allows one to obtain good agreement with the Zheleznyak integral model, and that single or two-exponential fits do not allow the Zheleznyak model to be reproduced accurately. We have also demonstrated that a proper setting of boundary conditions significantly improves the agreement between the Zheleznyak model and the three differential models.

Our model studies of the double-headed streamer have demonstrated that with the three-group Eddington, the three-group SP_3, or the three-exponential Helmholtz models, the calculated streamers are very similar to the one calculated using the classical Zheleznyak integral model. It is particularly interesting to note that the Eddington and SP_3 models, which are in principle only very well suited to situations in which photon absorption is sufficiently high, can be used to calculate very accurately the photoionization source term using a three-group approach even if some effective absorption coefficients in the model are small.

The comparison of the photoionization and ionization source terms for the studied case of strong uniform applied field indicates that photoionization only plays a role during the very early stage of the development of the streamer. These results indicate the need to conduct further studies for a streamer propagating in a weak electric field (less than the conventional breakdown field) in order to complete tests of the performance of the newly proposed photoionization models under the full range of applied field conditions. The related results will be presented in a separate dedicated paper.

In this work, we have also compared streamer modelling results obtained using different numerical techniques to solve the transport equations for charged particles: the Zalesak flux-corrected transport (FCT) method and the modified Scharfetter–Gummel (SG) algorithm. We have also utilized different techniques for solution of Poisson's field equation: the D03EBF module of the NAG Fortran library and the SOR method, which are used in conjunction with the FCT and SG transport algorithms, respectively. The results of solution of the same double-headed streamer problem obtained by the FCT method based on a 3rd order QUICKEST scheme and an upwind scheme, and by the modified SG algorithm demonstrate that both numerical techniques lead to accurate and consistent solutions of the streamer problem.

The results of accurate measurement of computational time involved in calculations using different photoionization models for the considered model streamer are presented, which indicate, in particular, that the computational times of the differential and optimized integral models for the model case considered in this study are of the same order. However, it is important to mention that a significant acceleration of the integral models in simple cases of single or double-headed streamers studied with these models to date has been possible due to introduction of moving meshes with variable cell sizes and employment of effective windowing and interpolation techniques. The details of related algorithms are presented in this paper. It is important to stress that the optimization of the integral model is rather complex and requires to be separately adapted to every new configuration studied. Conversely, the implementation of the photoionization models based on the differential equation approach is straightforward and simple. Furthermore, in the optimized integral approach the photoionization source term is calculated accurately only close to the streamer heads. For example, in the double-headed test-case, we have shown that in the optimized integral model the photoionization source term is not calculated accurately in the region between the streamer heads (see discussion of figure 12(*b*) in section 3.2). Conversely with the differential approaches the photoionization term is calculated accurately in the whole computation domain.

Although the different photoionization models are only used to model streamer discharges in air in this study, we expect that the models can be applied to evaluating the photoionization effects in other forms of plasma discharges in air. In addition, the extension of the photoionization models to other gases is possible if the information on all emission, absorption and photoionization coefficients of the studied gas is available.

The presented results document the range of applicability of the newly developed photoionization models and emphasize that the accurate formulation of boundary conditions represents an important task needed for a successful extension of the proposed formulations to two- and three-dimensional physical systems with obstacles of complex geometry (i.e. electrodes, dust particles, aerosols, etc), which are opaque for the photoionizing UV photons. We have demonstrated that accurate definition of the boundary conditions can be effectively introduced with the Zheleznyak integral model. For the Eddington model we have also demonstrated the performance of a set of boundary conditions consistent with the first order approximation of the radiative transfer equation. These boundary conditions are simple, fast to compute and easy to adapt to any configuration. The possibility of formulating such a consistent set of equations and boundary conditions based on radiative transfer physics is a significant advantage of the Eddington and SP_3 models in comparison with the Helmholtz model. In a future work similar boundary conditions for the SP_3 model will be derived and optimized.

We conclude by emphasizing that the actual advantage of differential models advanced in this paper in comparison with the integral model lies in the simplicity of implementation of this type of models, and in the unquestionable simplicity of extension of these models to complex two- and three-dimensional simulation geometries, involving, for example, propagation of multiple streamer heads in the same simulation domain, and the presence of obstacles on the streamer path (i.e. electrodes, dust particles, aerosols, etc).

Acknowledgments

The participation of V P Pasko and N Y Liu has been supported by the United States National Science Foundation under the NSF ATM-0134838 grant to Penn State University. This study was initiated during a sabbatical visit of V P Pasko to the EM2C Laboratory, Ecole Centrale Paris, France, and to the CPAT (LAPLACE) Laboratory, Université Paul Sabatier, Toulouse, France, in the Fall of 2006, which was partially supported by the Electrical Engineering Department of Penn State University and by Ecole Centrale Paris. The authors would like to thank Dr P Rivière (EM2C Laboratory) for helpful discussions.

Appendix: mathematical relationships between the Eddington, SP_3 and Helmholtz models

The three-group Eddington and SP_3 models presented in the main body of this paper have been derived on physical grounds from the general radiative transfer equation. These physics based models have certain advantages in comparison with the Helmholtz model, allowing in particular to formulate a consistent and computationally efficient set of equations and boundary conditions based on a radiative transfer theory (see section 2.3). It is useful, however, to bring to the attention of the readers that equation (15) of the Eddington model and equations (18) and (19) of the SP_3 model are Helmholtz equations. Therefore, as demonstrated below in this appendix, for these equations it is possible to derive effective representations of the $g(R)/p_{O_2}$ function of the type specified by equation (9) of the Helmholtz model described in section 2.2. The establishment of these mathematical relationships between Eddington, SP_3 and Helmholtz models is very useful for interpretation of the results presented in section 3.1, and evaluation of performance of the Eddington and SP_3 models in the general context of the quality of the fit of the $g(R)/p_{O_2}$ function given by equation (9) in comparison with the original $g(R)/p_{O_2}$ function of the Zheleznyak photoionization model specified by equation (3).

Each of the Helmholtz differential equations (8) is similar to equations for wave potentials commonly encountered in antenna theory in electromagnetics (Harrington 2001, p 77). On a conceptual level the electromagnetic problem corresponds to a case of purely imaginary λ_j values for which equation (7) would represent outgoing waves (Harrington 2001, p 80). In the photoionization problem the λ_j values are real, reflecting exponential spatial damping of the solutions due to the absorption of the photoionizing radiation. The appearance of the similar Helmholtz equations (15), (18) and (19) in the Eddington and improved Eddington approximations to the radiative transfer equation is also consistent with the above physical interpretation. In this appendix we demonstrate that the solutions of the Helmholtz, Eddington and SP_3 models can be represented in a mathematically equivalent form, however, all represent approximate solutions of the same problem, rely on different numerical values of the model coefficients and therefore generally do not lead to identical results.

In this context it is useful to recall that the Eddington and the Helmholtz models are simply based on different forms of approximation of the integral specified by equation (1). The original integral contains a difference of two exponents divided by R^3, the three-group Eddington model approximates the function under integral by a sum of three exponents divided by R^2 (section 2.3) and the three-exponential Helmholtz model approximates the same function by three exponents divided by R (section 2.2). If the problem is solved correctly all the approximations should lead to solutions consistent with S_{ph} (1).

In this appendix in order to distinguish between the coefficients involved in the Helmholtz (table 2) and the Eddington (table 3) models, we will use notations A_j^* ($cm^{-2}\,Torr^{-2}$), λ_j^* ($cm^{-1}\,Torr^{-1}$) and A_j ($cm^{-1}\,Torr^{-1}$), λ_j ($cm^{-1}\,Torr^{-1}$), for the Helmholtz and the Eddington models, respectively.

We observe that the Helmholtz equation (15) appearing as part of the development of the Eddington approximation are similar in structure to (8) and therefore have formal solutions of the type specified by (7). On these grounds, after simple algebraic manipulations, we can write the solution for the photoionization production rate satisfying equation (15) in the form

$$S_{ph}(\vec{r}) = \iiint_{V'} \frac{I(\vec{r}')p_{O_2}}{4\pi R^2}(p_{O_2}R)\sum_j 3A_j\lambda_j e^{-\sqrt{3}\lambda_j p_{O_2}R}\,dV'. \tag{A.1}$$

Alternatively, equation (13), representing the same $S_{ph}(\vec{r})$ before the approximation based in the isotropic part of the photon distribution function is applied (see section 2.3), can be written as

$$S_{ph}(\vec{r}) = \iiint_{V'} \frac{I(\vec{r}')p_{O_2}}{4\pi R^2}\sum_j A_j e^{-\lambda_j p_{O_2}R}\,dV'. \tag{A.2}$$

Having introduced $A_j^* = 3A_j\lambda_j$ and $\lambda_j^* = \sqrt{3}\lambda_j$, and remembering that in accordance with (9) and (14)

$$\frac{g(R)}{p_{O_2}} = (p_{O_2}R)\sum_j A_j^* e^{-\lambda_j^* p_{O_2}R} = \sum_j A_j e^{-\lambda_j p_{O_2}R} \tag{A.3}$$

it can be easily seen that equation (A.1) employs exactly the same form of approximation to the $g(R)/p_{O_2}$ function as used in the Helmholtz model. These relationships demonstrate mathematical equivalence between the three-exponential Helmholtz model based on equation (8) and the three-group Eddington approximation based on equation (15).

We note that taking the three-group Eddington parameters from table 3 and calculating the three-exponential Helmholtz model parameters using the above derived relationships $A_j^* = 3A_j\lambda_j$ and $\lambda_j^* = \sqrt{3}\lambda_j$ leads to the $g(R)/p_{O_2} = (p_{O_2}R)\sum_j A_j^* e^{-\lambda_j^* p_{O_2}R}$ function shown in figure A1 by the dot-dashed line, which does not agree with similar function shown in figure 2. Thus obtained A_j^* and λ_j^* are different from those given in table 2.

Alternatively, taking A_j^* and λ_j^* from table 2 and calculating $\lambda_j = \lambda_j^*/\sqrt{3}$ and $A_j = A_j^*/(3\lambda_j)$ leads to $g(R)/p_{O_2} = \sum_j A_j e^{-\lambda_j p_{O_2}R}$ shown in figure A1 by the dashed line, which significantly deviates from similar function shown in figure 3. Similarly to the previous case we note that thus obtained A_j and λ_j are different from those given in table 3.

These results demonstrate that although the two model formulations can be represented in a mathematically equivalent

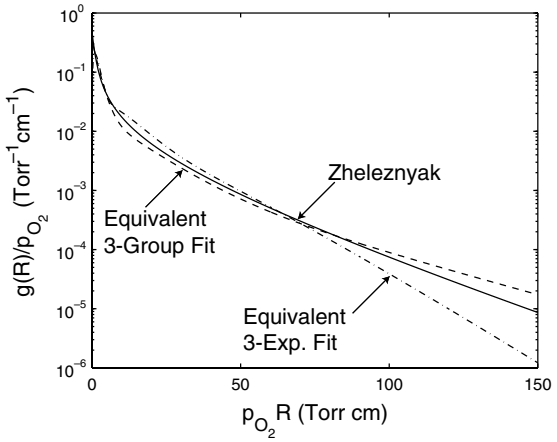

Figure A1. Solid line: the $g(R)/p_{O_2}$ function given by equation (3) from the model of Zheleznyak *et al* (1982). Dot-dashed line: equivalent three-exponential fit for the Helmholtz model obtained from the three-group Eddington approximation. Dashed line: equivalent three-group fit for the Eddington approximation based on three-exponential Helmholtz model.

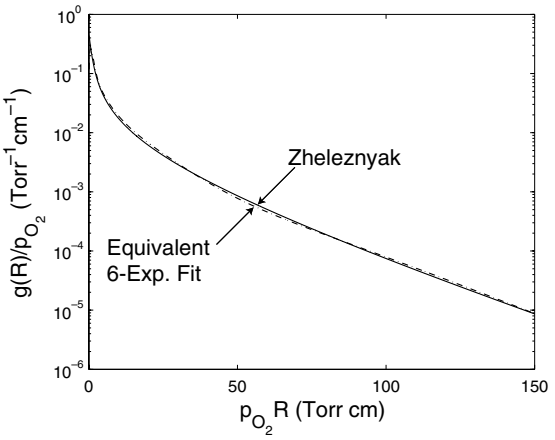

Figure A2. Solid line: The $g(R)/p_{O_2}$ function given by equation (3) from the model of Zheleznyak *et al* (1982). Dot-dashed line: Equivalent six-exponential fit for the Helmholtz model obtained from the three-group SP_3 model.

form, additional approximations involved in previous steps of the derivation of the Eddington model (i.e. related to the spherical harmonic expansion of the photon distribution function) lead to different numerical values of model coefficients and explain why results obtained from these two models are not identical.

It is interesting to note that since the three-group Eddington model is based on solutions of the Helmholtz equation (15) of the form (A.1) with $g(R)/p_{O_2}$ effectively given by dot-dashed line in figure A1, the discrepancies observed between the three-group Eddington approximation and the Zheleznyak model in figures 6(*c*) and (*d*) of section 3.1 can be directly linked to the discrepancies between the $g(R)/p_{O_2}$ and the Zheleznyak model at large $p_{O_2}R$ values in figure A1. The establishment of these relationships is therefore useful for evaluation of the performance of the Eddington model.

In view of the above mentioned mathematical relationships between the two models it might be tempting to replace the parameters of the Eddington model with the ones from the Helmholtz model providing a better fit. However, this step is not justified in the context of the rigorous development of the Eddington and the improved Eddington (SP_3) models, and as discussed in section 3.1 and further reiterated below in this appendix the SP_3 model takes full advantage of the original accurate fit specified by the parameters given in table 3 and leads to significantly improved solutions in comparison with the Eddington model.

We note that the Helmholtz equations (18) and (19) appearing as a part of the SP_3 model are similar in structure to (8) and have formal solutions of the type (7). By summing these solutions using equation (16), the corresponding photoionization rate (20) can be expressed in the form

$$S_{\rm ph}(\vec{r}) = \iiint_{V'} \frac{I(\vec{r}\,')p_{O_2}}{4\pi R^2}(p_{O_2}R)\sum_j A_j^* {\rm e}^{-\lambda_j^* p_{O_2} R}\,{\rm d}V' \tag{A.4}$$

with the corresponding six pairs of (A_j^*, λ_j^*) of the equivalent six-exponential Helmholtz model defined by $\lambda_1^* = \lambda_1/\kappa_1$, $\lambda_2^* = \lambda_2/\kappa_1$, $\lambda_3^* = \lambda_3/\kappa_1$, $\lambda_4^* = \lambda_1/\kappa_2$, $\lambda_5^* = \lambda_2/\kappa_2$, $\lambda_6^* = \lambda_3/\kappa_2$;

$$A_1^* = \lambda_1 A_1\gamma_2/(\kappa_1^2(\gamma_2-\gamma_1)),$$
$$A_2^* = \lambda_2 A_2\gamma_2/(\kappa_1^2(\gamma_2-\gamma_1)),$$
$$A_3^* = \lambda_3 A_3\gamma_2/(\kappa_1^2(\gamma_2-\gamma_1)),$$
$$A_4^* = -\lambda_1 A_1\gamma_1/(\kappa_2^2(\gamma_2-\gamma_1)),$$
$$A_5^* = -\lambda_2 A_2\gamma_1/(\kappa_2^2(\gamma_2-\gamma_1)),$$
$$A_6^* = -\lambda_3 A_3\gamma_1/(\kappa_2^2(\gamma_2-\gamma_1)).$$

Having taken the three-group Eddington parameters (A_j, λ_j) from table 3 and calculated the six-exponential Helmholtz model parameters using the above derived relationships leads to the $g(R)/p_{O_2} = (p_{O_2}R)\sum_j A_j^* {\rm e}^{-\lambda_j^* p_{O_2} R}$ function shown in figure A2 by the dot-dashed line, which is in substantially better agreement with the original Zheleznyak function in comparison with the similar equivalent three-exponential fit, obtained for the three-group Eddington model, shown by the dot-dashed line in figure A1. The good performance of the three-group SP_3 model in figures 6(*c*) and (*d*) of section 3.1 can be directly linked to the better agreement between the six-exponential $g(R)/p_{O_2}$ fit with the original Zheleznyak function in figure A2.

In summary, in this appendix we have demonstrated the mathematical equivalence of the Eddington, SP_3 and Helmholtz models. All solutions of these models can be written in essentially the same mathematical form, with differences between these models only arising from different numerical values of the model coefficients. The presented analysis demonstrates that the three-exponential Helmholtz model presented in section 2.2 is more accurate than the three-group Eddington model presented in section 2.3, in agreement with results presented in section 3.1. The presented analysis also demonstrates that the SP_3 model can be effectively represented in a mathematical form equivalent to the six-exponential Helmholtz model. This approach allows a simple interpretation of better performance of the three-group SP_3 model in comparison with the three-group Eddington model introduced in section 2.3, and in comparison with the three-exponential Helmholtz model presented in section 2.3, in agreement with the results presented in section 3.1.

References

Arrayás M, Ebert U and Hundsdorfer W 2002 Spontaneous branching of anode-directed streamers between planar electrodes *Phys. Rev. Lett.* **88** 174502(R) doi:10.1103/PhysRevLett.88.174502

Babaeva N Y and Naidis G V 1996 Two-dimensional modelling of positive streamer dynamics in non-uniform electric fields in air *J. Phys. D: Appl. Phys.* **29** 2423–31 doi:10.1088/0022-3727/29/9/029

Babaeva N Y and Naidis G V 1997 Dynamics of positive and negative streamers in air in weak uniform electric fields *IEEE Trans. Plasma Sci.* **25** 375–9

Babaeva N Y, Bhoj A N and Kushner M J 2006 Streamer dynamics in gases containing dust particles *Plasma Sources Sci. Technol.* **15** 591–602

Bastien F and Marode E 1979 The determination of basic quantities during glow-to-arc transition in a positive point-to-plane discharge *J. Phys. D: Appl. Phys.* **12** 249–63

Bazelyan E M and Raizer Y P 1998 *Spark Discharge* (New York, NY: Chemical Rubber Company Press)

Briels T M P, van Veldhuizen E M and Ebert U 2005 Branching of positive discharge streamers in air at varying pressures *IEEE Trans. Plasma Sci.* **33** 264–5

Briels T M P, Kos J, van Veldhuizen E M and Ebert U 2006 Circuit dependence of the diameter of pulsed positive streamers in air *J. Phys. D: Appl. Phys.* **39** 5201–10

Cummer S A, Jaugey N C, Li J B, Lyons W A, Nelson T E and Gerken E A 2006 Submillisecond imaging of sprite development and structure *Geophys. Res. Lett.* **33** L04104 doi:10.1029/2005GL024969

Dhali S K and Williams P F 1987 Two-dimensional studies of streamers in gases *J. Appl. Phys.* **62** 4696–707

Djakov A F, Bobrov Y K and Yourguelenas Y V 1998 Modeling of a positive streamer in air in a non-uniform external field *Physics and Technology of Electric Power Transmission* vol Book 1, ed A F Djakov pp 161–200 (Moscow: MPEI Publishers)

Djermoune D, Marode E and Ségur P 1995a Two dimensional modelling of a streamer induced discharge *Proc. 22th Int. Conf. on Phenomena in Ionized Gases (Hoboken, USA)* pp 33–4

Djermoune D, Samson S, Marode E and Ségur P 1995b A time resolved two dimensional modelling of the electrical behaviour and the chemical yield of the streamer induced discharge *Proc. 11th Int. Conf. on Gas Discharges and Their Applications (Chuo University, Tokyo, Japan)* pp 484–7

Ebert U, Montijn C, Briels T M P, Hundsdorfer W, Meulenbroek B, Rocco A and van Veldhuizen E M 2006 The multiscale nature of streamers *Plasma Sources Sci. Technol.* **15** S118–29

Franz R C, Nemzek R J and Winckler J R 1990 Television image of a large upward electric discharge above a thunderstorm system *Science* **249** 48

Gerken E A and Inan U S 2002 A survey of streamer and diffuse glow dynamics observed in sprites using telescopic imagery *J. Geophys. Res.* **107** 1344 doi:10.1029/2002JA009248

Gerken E A and Inan U S 2003 Observations of decameter-scale morphologies in sprites *J. Atmos. Sol.-Terr. Phys.* **65** 567–72 doi:10.1016/S1364-6826(02)00333-4

Gerken E A and Inan U S 2005 Streamers and diffuse glow observed in upper atmospheric electrical discharges *IEEE Trans. Plasma Sci.* **33** 282–3 doi:10.1109/TPS.2005.845010

Gerken E A, Inan U S and Barrington-Leigh C P 2000 Telescopic imaging of sprites *Geophys. Res. Lett.* **27** 2637–40

Hallac A, Georghiou G E and Metaxas A C 2003 Secondary emission effects on streamer branching in transient non-uniform short-gap discharges *J. Phys. D: Appl. Phys.* **36** 2498–509 doi:10.1088/0022-3727/36/20/011

Harrington R F 2001 Time-Harmonic Electromagnetic Fields (Pistcataway, NJ/New York: IEEE/Wiley)

Kulikovsky A A 1995 A more accurate Scharfetter–Gummel algorithm of electron transport for semiconductor and gas discharge simulation *Comput. Phys.* **119** 149–55

Kulikovsky A A 1997 Positive streamer between parallel plate electrodes in atmospheric pressure air *J. Phys. D: Appl. Phys.* **30** 441–50

Kulikovsky A A 2000 The role of photoionization in positive streamer dynamics *J. Phys. D: Appl. Phys.* **33** 1514–24

Kunhardt E E and Tzeng Y 1988 Development of an electron avalanche and its transition into streamers *Phys. Rev.* A **38** 1410–21

Li C, Brok W J M, Ebert U and van der Mullen J J A M 2007 Deviations from the local field approximation in negative streamer heads *J. Appl. Phys.* **101** 123305

Liu N Y and Pasko V P 2004 Effects of photoionization on propagation and branching of positive and negative streamers in sprites *J. Geophys. Res.* **109** A04301 doi:10.1029/2003JA010064

Liu N Y and Pasko V P 2005 Molecular nitrogen LBH band system far-UV emissions of sprite streamers *Geophys. Res. Lett.* **32** L05104 doi:10.1029/2004GL022001

Liu N Y and Pasko V P 2006 Effects of photoionization on similarity properties of streamers at various pressures in air *J. Phys. D: Appl. Phys.* **39** 327–34 doi:10.1088/0022-3727/39/2/013

Liu N Y *et al* 2006 Comparison of results from sprite streamer modeling with spectrophotometric measurements by ISUAL instrument on FORMOSAT-2 satellite *Geophys. Res. Lett.* **33** L01101 doi:10.1029/2005GL024243

Loeb L B and Meek J M 1940 The mechanism of spark discharge in air at atmospheric pressure *J. Appl. Phys.* **11** 438–47

Luque A, Ebert U, Montijn C and Hundsdorfer W 2007 Photoionization in negative streamers: Fast computations and two propagation modes *Appl. Phys. Lett.* **90** 081501 doi:10.1063/1.2435934

Lyons W A 2006 The meteorology of transient luminous events—an introduction and overview *Sprites, Elves and Intense Lightning Discharges* (*NATO Science Series II: Mathematics, Physics and Chemistry* vol 225) ed M Füllekrug *et al* (Heidleberg, Germany: Springer) pp 19–56

McHarg M G, Stenbaek-Nielsen H C and Kammae T 2007 Streamer development in sprites *Geophys. Res. Lett.* **34** L06804 doi:10.1029/2006GL027854

Modest M 2003 *Radiative Heat Transfer* 2nd edn (New York: Academic)

Morrow R and Lowke J J 1997 Streamer propagation in air *J. Phys. D: Appl. Phys.* **30** 614–27

Naidis G V 1997 Effects of nonlocality on the dynamics of streamers in positive corona discharges *Tech. Phys. Lett.* **23** 493–4

Naidis G V 2006 On photoionization produced by discharges in air *Plasma Sources Sci. Technol.* **15** 253–5

Neubert T 2003 On sprites and their exotic kin *Science* **300** 747–9

Pancheshnyi S V, Starikovskaia S M and Starikovskii A Y 2001 Role of photoionization processes in propagation of cathode-directed streamer *J. Phys. D: Appl. Phys.* **34** 105–15

Pancheshnyi S V, Nudnova M and Starikovskii A Y 2005 Development of a cathode-directed streamer discharge in air at different pressures: experiment and comparison with direct numerical simulation *Phys. Rev.* E **71** 016407 doi:10.1103/PhysRevE.71.01640

Pasko V P 2007 Red sprite discharges in the atmosphere at high altitude: the molecular physics and the similarity with laboratory discharges *Plasma Sources Sci. Technol.* **16** S13–29 doi:10.1088/0963-0252/16/1/S02

Pasko V P, Inan U S and Bell T F 1998 Spatial structure of sprites *Geophys. Res. Lett.* **25** 2123–6

Penney G W and Hummert G T 1970 Photoionization measurements in air oxygen, and nitrogen *J. Appl. Phys.* **41** 572–7

Pomraning G 1973 *The Equations of Radiation Hydrodynamics* (New York: Pergamon)

Raizer Y P 1991 *Gas Discharge Physics* (New York, NY: Springer)

Rocco A, Ebert U and Hundsdorfer W 2002 Branching of negative streamers in free flight *Phys. Rev.* E **66** 035102(R) doi:10.1103/PhysRevE.66.035102

Ségur P, Bourdon A, Marode E, Bessières D and Paillol J H 2006 The use of an improved Eddington approximation to facilitate the calculation of photoionization in streamer discharges *Plasma Sources Sci. Technol.* **15** 648–60

Sentman D D, Wescott E M, Osborne D L, Hampton D L and Heavner M J 1995 Preliminary results from the Sprites94 campaign: red sprites *Geophys. Res. Lett.* **22** 1205–8

Stanley M, Krehbiel P, Brook M, Moore C, Rison W and Abrahams B 1999 High speed video of initial sprite development *Geophys. Res. Lett.* **26** 3201–4

Stenbaek-Nielsen H C, McHarg M G, Kanmae T and Sentman D D 2007 Observed emission rates in sprite streamer heads *Geophys. Res. Lett.* **34** L11105 doi:10.1029/2007GL029881

Taine J and Soufiani A 1999 Gas IR radiative properties: from spectroscopic data to approximate models *Advances in Heat Transfer* vol 33 ed J Hartnett and T Irvine (San Diego, CA: Academic) pp 295–414

Tardiveau P and Marode E 2003 Point-to-plane discharge dynamics in the presence of dielectric droplets *J. Phys. D: Appl. Phys.* **36** 1204–11

Tardiveau P, Marode E, Agneray A and Cheaib M 2001 Pressure effects on the development of an electric discharge in non-uniform fields *J. Phys. D: Appl. Phys.* **34** 1690–6

Teich T H 1967 Emission gasionisierender strahlung aus electronenlawinen: I. Meßanordnung und Meßverfahren Messungen in Sauerstoff *Z. Phys.* **199** 378–94

van Veldhuizen E M (ed) 2000 *Electrical Discharges for Environmental Purposes: Fundamentals and Applications* (New York: Nova Science)

Vitello P A, Penetrante B M and Bardsley J N 1994 Simulation of negative-streamer dynamics in nitrogen *Phys. Rev.* E **49** 5574–98

Wu C and Kunhardt E E 1988 Formation and propagation of streamers in N_2 and N_2–SF_6 mixtures *Phys. Rev.* A **37** 4396–406

Zalesak S T 1979 Fully multidimensional flux-corrected transport algorithms for fluids *J. Comput. Phys.* **31** 335–62

Zheleznyak M B, Mnatsakanyan A K and Sizykh S V 1982 Photoionization of nitrogen and oxygen mixtures by radiation from a gas discharge *High Temp.* **20** 357–62